

Review

An integrative model of respiratory and cardiovascular control in sleep-disordered breathing[☆]

Limei Cheng, Olga Ivanova, Hsing-Hua Fan, Michael C.K. Khoo*

Biomedical Engineering Department, University of Southern California, DRB-140, University Park, Los Angeles, CA 90089-1111, USA

ARTICLE INFO

Article history:
Accepted 3 June 2010

Keywords:

Physiological model simulation
Autonomic pathways and reflexes
Sleep regulation
Obstructive sleep apnoea
Cheyne–Stokes respiration
Cardiorespiratory interactions

ABSTRACT

While many physiological control models exist in the literature, none thus far has focused on characterizing the interactions among the respiratory, cardiovascular and sleep–wake regulation systems that occur in sleep-disordered breathing. The model introduced in this study integrates the autonomic control of the cardiovascular system, chemoreflex and state-related control of respiration, including respiratory and upper airway mechanics, along with a model of circadian and sleep–wake regulation. The integrative model provides realistic predictions of the physiological responses under a variety of conditions including: the sleep–wake cycle, hypoxia-induced periodic breathing, Cheyne–Stokes respiration in chronic heart failure, and obstructive sleep apnoea (OSA). It can be used to investigate the effects of a variety of interventions, such as isocapnic and hypercapnic and/or hypoxic gas administration, the Valsalva and Mueller maneuvers, and the application of continuous positive airway pressure on OSA subjects. By being able to delineate the influences of the various interacting physiological mechanisms, the model is useful in providing a more lucid understanding of the complex dynamics that characterize state-cardiorespiratory control in the different forms of sleep-disordered breathing.

© 2010 Elsevier B.V. All rights reserved.

1. Introduction

Many simulation models of the cardiovascular and respiratory systems have been published in the past several decades (Coleman and Randall, 1983; Dickinson, 1977; Grodins, 1959; Grodins et al., 1954; Khoo and Yamashiro, 1989; Madwed et al., 1989; Milhorn et al., 1965; Ursino and Magosso, 2003), starting with the highly simplified models proposed by Grodins et al. (1954). For instance, Grodins' early electrical analog of the cardiovascular system (1959) was largely an “uncontrolled” model, consisted of only 2 linear resistors and 4 compliances, along with flow sources that implemented the Frank–Starling mechanism. Subsequent models became more realistic through the incorporation of progressively more functional components (Coleman and Randall, 1983; Dickinson, 1977; Ursino and Magosso, 2003). As well, many models were designed to solve specific issues in cardiorespiratory physiology. As such, these models focused primarily on the functional characterization of the pertinent components of these systems while capturing as realistically as necessary the detailed feature in these components. Some examples include the

recent sophisticated models that provide very detailed mathematical representations of the structure and function of the heart (McCulloch et al., 1998) and lungs (Tawhai et al., 2004). While most models have addressed the cardiovascular and respiratory systems separately, only a subset have examined the interactions between these systems (Bai et al., 1997; Liang and Liu, 2006; Lu et al., 2001). While existing models are capable of characterizing the responses of the cardiovascular and respiratory systems to a wide range of interventions or conditions, very few have been developed for the simulation of the physiological response to sleep onset or the effect of circadian rhythms (Khoo et al., 1991; Stephenson, 2004). Certainly, none have addressed the integrated cardiovascular and respiratory responses that accompany normal or pathological sleep.

It has become widely recognized that the cardiovascular consequences of sleep-related breathing disorders, such as the obstructive sleep apnoea syndrome (OSAS) and Cheyne–Stokes respiration (CSR) can be quite profound (Bradley and Floras, 2003a, 2003b; Leung and Bradley, 2001). During both central and obstructive apnoea, absence of inspiratory airflow results in asphyxia, which subsequently stimulates breathing through the chemoreflexes and triggers a transient arousal from sleep. In OSAS, the arousal also leads to restoration of upper airway patency. These large fluctuations in chemoreflex and sleep state-related stimuli also produce concomitant changes in outflow in autonomic branches. There is accumulating evidence that chronic exposure to these repetitive swings in autonomic outflow and intermittent

[☆] This paper is part of a special issue entitled “Central cardiorespiratory regulation: physiology and pathology”, guest-edited by Thomas E. Dick and Paul M. Pilowsky.

* Corresponding author at: 1042 Downey Way, Denney Research Center Room 140, Los Angeles, CA 90089, USA. Tel.: +1 213 740 0347; fax: +1 213 821 3897.

E-mail address: khoo@bmsr.usc.edu (M.C.K. Khoo).

hypoxia can lead ultimately to the development of systemic hypertension, heart failure, myocardial infarction and stroke (Leung and Bradley, 2001; Stephenson, 2004).

Present knowledge about the mechanisms that link sleep-disordered breathing to cardiovascular disease remains incomplete. The multifactorial dynamics and closed-loop aspects of the physiological events that underlie respiratory and state instability during sleep apnoea make it difficult to distinguish cause from effect under such conditions. By employing a mathematical modeling approach, it is possible to extricate the influences of the various interacting physiological mechanisms and thus attain a more lucid understanding of how they contribute to the complex dynamics that characterize cardiorespiratory control in the different forms of sleep-disordered breathing, such as OSAS and CSR. Subsequently, comparing the model predictions to the features extracted from empirical data provides insight into what the limitations of the current understanding are and what future experiments could be performed to address those limitations. This information can potentially be used to facilitate the identification of particular physiological defects, and the prediction or evaluation of specific outcomes for a given therapy.

In this paper, we introduce an integrative model which incorporates the essential features from existing submodels of cardiovascular, respiratory and sleep regulation and allows us to examine the interactions among these subsystems. The primary purpose for developing this integrative model is to provide the capability of performing virtual experiments and computer simulations of cardiorespiratory interactions under conditions of changing sleep–wake state as well as a variety of interventions, such as hypoxic gas administration, Valsalva and Mueller maneuvers, application of continuous positive airway pressure (CPAP), and Cheyne–Stokes respiration during sleep. The inclusion of a sleep regulation model allows simulations to be executed over time scales that span multiple sleep–wake cycles in months or even years.

The integrative model takes the form of a software package named “PNEUMA”. PNEUMA is implemented using SIMULINK®/MATLAB® (The Mathworks, Natick, MA), which provides a graphical environment that allows users to design the model components from built-in blocks or user defined functions, thus allowing the software to be executed across multiple computer platforms. The model code and supporting materials, including a user manual, are freely available to the research community. More information about the structure and implementation of the model can be downloaded from the USC Biomedical Simulations Resource website: <http://bmsr.usc.edu/Software/PNEUMA/PNEUMA.html>.

2. Methods

The model is developed by employing a hierarchical structure so that the degree of complexity at each level of organization is tailored appropriately to the investigation of the physiological processes at that level. This allows the overall model to be represented in a compact and efficient manner. At the highest level of organization, PNEUMA consists of four major interconnected “blocks”: (a) the first representing the respiratory subsystem; (b) the second representing the cardiovascular subsystem; (c) the third representing central neural control; and (d) the last representing the sleep mechanism. The respiratory subsystem includes upper airway dynamics, respiratory mechanics, gas exchange, and circulatory transport/mixing of blood gases. The cardiovascular subsystem contains the pulsating heart and hemodynamics of pulmonary and systemic circulations with its peripheral circulations, the automaticity of the Sino-Atrial (SA) node, the carotid baroreflex regulation, and the local blood flow control in the peripheral cir-

culations. The central neural control system consists of the ventilatory controller, a variable respiratory rhythm generator, autonomic control, several key reflexes: chemoreflex, baroreflex and lung stretch reflex, and cardiorespiratory interactions that include respiratory sinus arrhythmia, pleural pressure modulation and central nervous system (CNS) response to arterial P_{O_2} and arterial P_{CO_2} in the cerebral blood flow that are necessary to model sympathetic and parasympathetic branches of autonomic control. The sleep mechanism counts for both circadian and ultradian rhythms. A schematic diagram of the model is displayed in Fig. 1.

In this section, the major features that characterize these subsystems are highlighted, as well as key assumptions employed in the modeling process. All model equations are given in Appendix A. A glossary of the model variables and parameters, as well as their nominal values, is provided in Table 1. To facilitate the flow of logic in the presentation of the model below, we have found it useful to include the characterizations of the cardiovascular- and respiratory-related components of the central neural control block in the descriptions of the cardiovascular and respiratory subsystems, respectively.

2.1. Respiratory subsystem and its central neural control subsystem (see Appendix Eqs. (A.1)–(A.40))

The respiratory subsystem allows simulation of both mechanical and gas exchange characteristics of breathing. The compartment representing respiratory mechanics receives input (total respiratory drive) from the central neural control subsystem and generates the airflow based on the curvilinear relationship between the respiratory muscles and the lung volume according to the Younes model (Riddle and Younes, 1981). Pleural and alveolar pressures are obtained by solving the lumped-parameter equations that take into consideration the viscous and elastic properties of the chest wall and lung tissues (Schuessler et al., 1997). Compared to other published models, the advantages of our model are that: (1) it is able to generate pleural pressure by itself such that the model does not need any external input, and (2) it is able to run by itself in closed-loop mode (Lu et al., 2001).

The gas exchange section consists of a tidal-breathing single-alveolar compartment lung model connected to a dead space that is comprised of 5 small serial compartments (Khuo, 1990). The nonlinear blood–gas dissociation curves, which also incorporate the Bohr–Haldane effects, are based on those published by Spencer et al. (1979). Mixing in the heart and vasculature is modeled after empirical transfer functions derived by Lange et al. (1966). Brain P_{CO_2} , which affects the central chemoreflex response, is computed from the first-order differential equation proposed by Read and Leigh (1967). Gas exchange that occurs outside of the lungs and the brain is modeled as taking place in a single body tissues compartment (Khuo, 1990).

The ventilatory controller incorporates both central and peripheral chemoreceptor contributions. The central component is assumed to respond to only brain P_{CO_2} , while the peripheral component is influenced by arterial P_{CO_2} and P_{O_2} and their multiplicative interaction (Khuo et al., 1991). The total ventilatory drive is assumed to be the sum of the central and peripheral chemoreflex components along with an additive state-related component which is modulated by a sleep–wake state index (SI). The output of the ventilator controller feeds into a series of control blocks that represents the neural processes responsible for short-term potentiation (STP) or the “ventilatory afterdischarge” (Dempsey et al., 2002). Our model of STP consists of an initial block that nonlinearly transforms the input from the ventilatory controller and sends the resulting output into a linear dynamic system composed of a static gain placed in parallel with a leaky integrator. The static gain is responsible for the direct effect of STP, converting part of the input

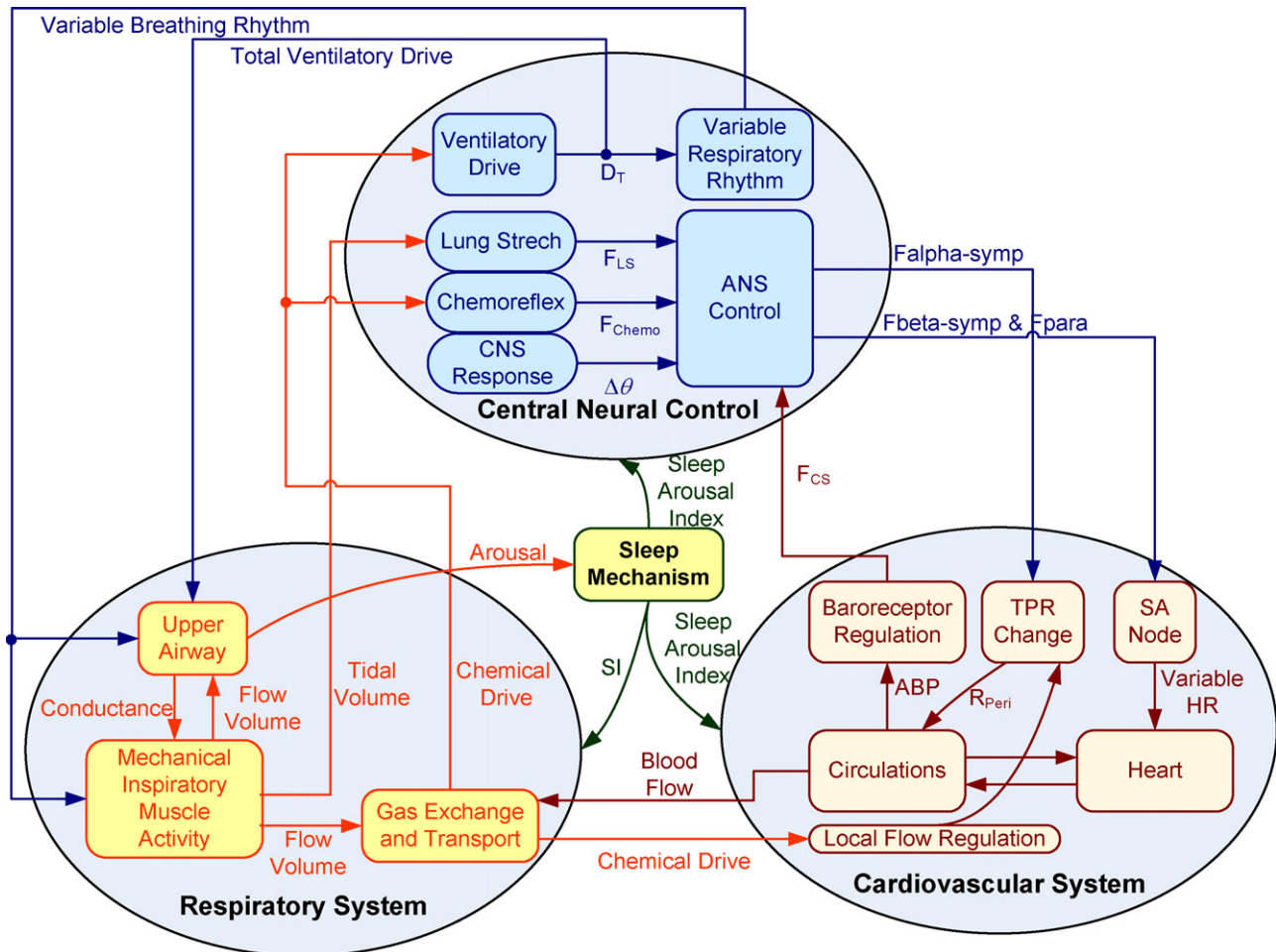


Fig. 1. Schematic diagram of the integrative model of cardiovascular and respiratory interactions with sleep-wake state control.

instantaneously into a portion of the response. The leaky integrator contributes to the relatively slower afterdischarge, which decays with a time constant of approximately 40 s. A nonlinear process with threshold and saturation is placed at the output end of the STP model. Finally, the “filtered” total ventilatory drive is decomposed into tidal volume and respiratory rhythm (breath period) components using the model proposed by Duffin et al. (2000). The continuously-varying breath period component is converted into stair-like respiration rate signal, so that breathing frequency is constant at each breath, using an integral pulse frequency modulation (IPFM) model, similar to what is used for generating heart period.

An important feature of the respiratory subsystem not derived from existing models is the component representing upper airway dynamics. Although sophisticated finite-element models of upper airway mechanics exist (Huang et al., 2005), for the purposes of this study, we opted for computational simplicity by employing a lumped-parameter model. Here, upper airway conductance Y_{ua} (the inverse of upper airway resistance) is assumed to be a linear function of the upper airway cross-sectional area, which in turn is dependent on the local transmural upper airway pressure (P_{ua}). When P_{ua} is less than ambient pressure but greater than the critical pressure (P_{crit}), Y_{ua} is a linear function of P_{ua} with a slope that depends on P_{crit} . When P_{ua} is equal to or greater than ambient pressure, the upper airway is fully open and thus upper airway conductance assumes its maximum value. When P_{ua} is equal to or less than the critical pressure P_{crit} , the upper airway collapses and the corresponding conductance becomes zero (or equivalently, upper airway resistance becomes infinite). P_{crit} itself is a function

of sleep-wake state (SI): in wakefulness, P_{crit} takes on a negative value, but in sleep, P_{crit} becomes less negative. Thus, upper airway conductance is nonlinearly dependent on sleep-wake state, changing between higher values in wakefulness and lower values during sleep. The upper airway sensitivity parameter, S_{ua} , controls the dependence of P_{crit} on SI. In the simulated subject with OSAS, S_{ua} is assigned a value substantially higher than its default value in the control case.

2.2. Cardiovascular subsystem and its central neural control subsystem (Appendix Eqs. (A.41)–(A.73))

The cardiovascular subsystem is capable of simulating the pulsatile nature of the heart and blood flow through the pulmonary and systemic circulations. Included in the model are descriptions of atria-ventricular mechanics, hemodynamics of the systemic and pulmonary circulations, SA node, change of total peripheral resistance and baroreflex. The models of the pulsatile heart, pulmonary circulation and systemic circulation, splanchnic, extrasplanchnic, muscular, coronary and cerebral peripheral circulations are based largely on the work of Ursino but have been modified in terms of different sleep-wake states (Ursino, 1998; Ursino and Magosso, 2000).

The SA node is modeled as a simple pacemaker that receives parasympathetic and beta-sympathetic inputs, but the gain of which is modulated by the sleep index and arousal index. An IPFM model is used to convert the continuous variable representing instantaneous heart rate (the driving signal) into a discrete period

Table 1
PNEUMA simulation parameters and initial conditions.

Parameter	Definition	Values	Units	Source
Cardiovascular system				
Resistances				
R_{PA}	Pulmonary arterial flow resistance	0.023	mmHg s/mL	Ursino (1998)
R_{PP}	Pulmonary peripheral flow resistance	0.0894	mmHg s/mL	Ursino (1998)
R_{PV}	Pulmonary venous flow resistance	0.0056	mmHg s/mL	Ursino (1998)
R_{SA}	Systemic arterial flow resistance	0.06	mmHg s/mL	Ursino and Magosso (2000)
R_{SP}	Splanchnic peripheral flow resistance	3.307	mmHg s/mL	Ursino and Magosso (2000)
R_{EP}	Extrasplanchnic peripheral resistance	3.52	mmHg s/mL	Ursino and Magosso (2000)
R_{MPN}	Skeletal muscle peripheral flow resistance	4.48	mmHg s/mL	Ursino and Magosso (2000)
R_{BPN}	Cerebral peripheral flow resistance	6.57	mmHg s/mL	Ursino and Magosso (2000)
R_{HPN}	Coronary peripheral flow resistance	19.71	mmHg s/mL	Ursino and Magosso (2000)
R_{SV}	Splanchnic venous flow resistance	0.038	mmHg s/mL	Ursino and Magosso (2000)
R_{EV}	Extrasplanchnic venous resistance	0.04	mmHg s/mL	Ursino and Magosso (2000)
R_{MV}	Skeletal muscle venous flow resistance	0.05	mmHg s/mL	Ursino and Magosso (2000)
R_{BV}	Cerebral venous flow resistance	0.075	mmHg s/mL	Ursino and Magosso (2000)
R_{HV}	Coronary venous flow resistance	0.224	mmHg s/mL	Ursino and Magosso (2000)
$R_{VC,0}$	Nominal vena cava flow resistance	0.025	mmHg s/mL	Model
R_{LA}	Left atrial flow resistance	0.0025	mmHg s/mL	Ursino (1998)
R_{RA}	Right atrial flow resistance	0.0025	mmHg s/mL	Ursino (1998)
Compliances				
C_{PA}	Pulmonary arterial compliances	0.76	mL/mmHg	Ursino (1998)
C_{PP}	Pulmonary peripheral compliances	5.8	mL/mmHg	Ursino (1998)
C_{PV}	Pulmonary venous compliances	25.37	mL/mmHg	Ursino (1998)
C_{SA}	Systemic arterial compliances	0.28	mL/mmHg	Ursino and Magosso (2000)
C_{SP}	Splanchnic peripheral compliances	2.05	mL/mmHg	Ursino and Magosso (2000)
C_{EP}	Extrasplanchnic peripheral compliances	0.668	mL/mmHg	Ursino and Magosso (2000)
C_{MP}	Skeletal muscle peripheral compliances	0.525	mL/mmHg	Ursino and Magosso (2000)
C_{BP}	Cerebral peripheral compliances	0.358	mL/mmHg	Ursino and Magosso (2000)
C_{HP}	Coronary peripheral compliances	0.119	mL/mmHg	Ursino and Magosso (2000)
C_{SV}	Systemic venous compliances	61.11	mL/mmHg	Ursino and Magosso (2000)
C_{EV}	Extrasplanchnic venous compliances	20	mL/mmHg	Ursino and Magosso (2000)
C_{MV}	Skeletal muscle venous compliances	15.71	mL/mmHg	Ursino and Magosso (2000)
C_{BV}	Cerebral venous compliances	10.71	mL/mmHg	Ursino and Magosso (2000)
C_{HV}	Coronary venous compliances	3.57	mL/mmHg	Ursino and Magosso (2000)
C_{LA}	Left atrial compliances	19.23	mL/mmHg	Ursino (1998)
C_{RA}	Right atrial compliances	31.25	mL/mmHg	Ursino (1998)
Inertances				
L_{PA}	Pulmonary arterial inertance	0.00018	mmHg s ² /mL	Ursino (1998)
L_{SA}	Systemic arterial inertance	0.00022	mmHg s ² /mL	Ursino (1998)
Unstressed volume				
V_{UPA}	Pulmonary arterial unstressed volume	0	mL	Ursino (1998)
V_{UPP}	Pulmonary peripheral unstressed volume	123	mL	Ursino (1998)
V_{UPV}	Pulmonary venous unstressed volume	120	mL	Ursino (1998)
V_{USA}	Systemic arterial unstressed volume	0	mL	Ursino and Magosso (2000)
V_{USP}	Splanchnic peripheral unstressed volume	274.4	mL	Ursino and Magosso (2000)
V_{UEP}	Extrasplanchnic peripheral unstressed volume	134.64	mL	Ursino and Magosso (2000)
V_{UMP}	Skeletal muscle peripheral unstressed volume	105.8	mL	Ursino and Magosso (2000)
V_{UBP}	Cerebral peripheral unstressed volume	72.13	mL	Ursino and Magosso (2000)
V_{UHP}	Coronary peripheral unstressed volume	24	mL	Ursino and Magosso (2000)
V_{USV}	Splanchnic venous unstressed volume	1121	mL	Ursino and Magosso (2000)
V_{UEV}	Extrasplanchnic venous unstressed volume	550	mL	Ursino and Magosso (2000)
V_{UMV}	Skeletal muscle venous unstressed volume	432.14	mL	Ursino and Magosso (2000)
V_{UBV}	Cerebral venous unstressed volume	294.64	mL	Ursino and Magosso (2000)
V_{UHV}	Coronary venous unstressed volume	98.21	mL	Ursino and Magosso (2000)
$V_{VC,0}$	Vena cava unstressed volume	130	mL	Model
V_{ULA}	Left atrial unstressed volume	25	mL	Ursino (1998)
V_{URA}	Right atrial unstressed volume	25	mL	Ursino (1998)
V_{ULV}	Left ventricular unstressed volume	16.77	mL	Ursino (1998)
V_{URV}	Right ventricular unstressed volume	40.88	mL	Ursino (1998)
Vena cava				
$K_{f,vc}$	Gain for vena cava flow resistance	0.001	mmHg s/mL	Lu et al. (2001)
$V_{vc,max}$	Maximum volume of vena cava	350	mL	Lu et al. (2001)
$V_{vc,min}$	Minimum volume of vena cava	50	mL	Lu et al. (2001)
D_1	Parameter for P – V curve of vena cava	0.3855	mmHg	Model
D_2	Parameter for P – V curve of vena cava	–5	mmHg	Lu et al. (2001)
K_1_{vc}	Parameter for P – V curve of vena cava	0.15	mmHg	Lu et al. (2001)
K_2_{vc}	Parameter for P – V curve of vena cava	0.4	mmHg	Lu et al. (2001)
Respiratory system				
Pleural pressure and alveolar pressure				
R_{CW}	Chest wall resistance	1.03	cmH ₂ O s/L	Schuessler et al. (1997)
R_{LT}	Lung transmural resistance	1.69	cmH ₂ O s/L	Schuessler et al. (1997)
R_{AW}	Airway wall resistance	1.016	cmH ₂ O s/L	Model

Table 1 (Continued)

Parameter	Definition	Values	Units	Source
E_{cw}	Chest wall elastance	5	cmH ₂ O/L	Schuessler et al. (1997)
E_{LT}	Lung transmural elastance	5	cmH ₂ O/L	Schuessler et al. (1997)
$k_{1,aw}$	Constant for upper airway pressure	1.85	cmH ₂ O s ² /L ²	Schuessler et al. (1997)
$k_{2,aw}$	Constant for upper airway pressure	0.43	cmH ₂ O s ² /L ²	Schuessler et al. (1997)
Gas exchange and transport				
Dead space				
$Dead_{(i),CO_2IC}$	Initial condition for i^{th} CO ₂ dead space	39.562	L	Khoo (1990)
$Dead_{(i),CO_2IC}$	Initial condition for i^{th} CO ₂ dead space	39.674	L	Khoo (1990)
$Dead_{(i),CO_2IC}$	Initial condition for i^{th} CO ₂ dead space	39.813	L	Khoo (1990)
$Dead_{(i),CO_2IC}$	Initial condition for i^{th} CO ₂ dead space	40.006	L	Khoo (1990)
$Dead_{(i),O_2IC}$	Initial condition for i^{th} O ₂ dead space	104.36	L	Khoo (1990)
$Dead_{(i),O_2IC}$	Initial condition for i^{th} O ₂ dead space	104.23	L	Khoo (1990)
$Dead_{(i),O_2IC}$	Initial condition for i^{th} O ₂ dead space	104.05	L	Khoo (1990)
$Dead_{(i),O_2IC}$	Initial condition for i^{th} O ₂ dead space	103.8	L	Khoo (1990)
$V_{d(i)}$	i^{th} dead space volume ($i = \{1, \dots, 4\}$)	0.03	L	Khoo (1990)
P_{I,CO_2}	Inspiratory CO ₂ partial pressure	0	Torr	Khoo (1990)
P_{I,O_2}	Inspiratory O ₂ partial pressure	150	Torr	Khoo (1990)
V'_t	Respiratory flow	Variable	L/s	Model
V_t	Tidal volume	Variable	L	Model
P_{dO_2}	Dead space O ₂ partial pressure	Variable	Torr	Model
P_{dCO_2}	Dead space CO ₂ partial pressure	Variable	Torr	Model
Alveolar gas exchange				
V_{CO_2}, V_{lCO_2}	Lungs storage volume for CO ₂	3	L	Khoo (1990)
V_{O_2}, V_{lO_2}	Lungs storage volume for O ₂	2.5	L	Khoo (1990)
P_{ACO_2IC}	Initial condition for partial CO ₂ pressure	40.943	Torr	Khoo (1990)
P_{AO_2IC}	Initial condition for partial O ₂ pressure	102.52	Torr	Khoo (1990)
P_{ACO_2}	Alveolar CO ₂ partial pressure	Variable	Torr	Model
P_{AO_2}	Alveolar O ₂ partial pressure	Variable	Torr	Model
P_{alv}	Alveolar partial gas pressure	Variable	Torr	Model
Q	Blood flow	Variable	L/s	Model
Cardiovascular transport				
τ_{chemo}	Peripheral chemoreceptors delay time constant	2	s	Khoo (1990)
T_1	Time constant for cardiovascular mixing	1	s	Khoo (1990)
T_2	Time constant for cardiovascular mixing	2	s	Khoo (1990)
T_a	Lung to chemoreceptor circulation delay	Variable	s	Lange et al. (1966)
$LCTV_0$	Lung to chemoreceptor transportation vascular volume constant	0.588	L	Lange et al. (1966)
$P_{aO_2_firstIC}$	Initial condition for first-order P_{aO_2} system	0.3557	Torr	Khoo (1990)
$P_{aO_2_secondIC}$	Initial condition for second order P_{aO_2} system	103.14	Torr	Khoo (1990)
$P_{aCO_2_firstIC}$	Initial condition for first-order P_{aCO_2} system	-0.2465	Torr	Khoo (1990)
$P_{aCO_2_secondIC}$	Initial condition for second order P_{aCO_2} system	40.393	Torr	Khoo (1990)
$P_{aO_2_delayIC}$	Initial condition for O ₂ convection	103.12	Torr	Khoo (1990)
$P_{aCO_2_delayIC}$	Initial condition for CO ₂ convection	40.445	Torr	Khoo (1990)
P_{aCO_2}	CO ₂ partial pressure	Variable	Torr	Model
P_{aO_2}	O ₂ partial pressure	Variable	Torr	Model
Cardiovascular dissociation				
$C1$	Maximum concentration of hemoglobin-bound oxygen	9	ml/ml	Khoo (1990)
$C2$	Maximum carbon dioxide concentration	87	ml/ml	Khoo (1990)
$a1$	Parameter in O ₂ dissociation equation	0.3836	Dimensionless	Spencer et al. (1979)
$a2$	Parameter in CO ₂ dissociation equation	1.819	Dimensionless	Spencer et al. (1979)
$\alpha1$	Parameter in O ₂ dissociation equation	0.02598	Dimensionless	Spencer et al. (1979)
$\alpha2$	Parameter in CO ₂ dissociation equation	0.05591	Dimensionless	Spencer et al. (1979)
$K1$	Parameter in O ₂ dissociation equation	13	Dimensionless	Spencer et al. (1979)
$K2$	Parameter in CO ₂ dissociation equation	194.4	Dimensionless	Spencer et al. (1979)
$\beta1$	Parameter in O ₂ dissociation equation	0.012275	Dimensionless	Spencer et al. (1979)
$\beta2$	Parameter in CO ₂ dissociation equation	0.03255	Dimensionless	Spencer et al. (1979)
$S_{aO_2_delayIC}$	Initial condition for oxygen saturation delay	98.92	s	Spencer et al. (1979)
Brain compartment				
MR_{bCO_2}	Metabolic production rate for CO ₂ in the brain tissue	0.0517	1/s STPD	Khoo (1990)
S_{CO_2}	Dissociation slope for CO ₂ in the blood	0.0043	ml/(ml Torr)	Khoo (1990)
S_{bCO_2}	Dissociation slope for CO ₂ in the brain tissue	0.36	ml 100 g ⁻¹ /Torr	Khoo (1990)
P_{bCO_2IC}	Initial condition for partial CO ₂ pressure from the brain	48.538	Torr	Khoo (1990)
Body tissues compartment				
V_{iCO_2}	Body tissue storage volume for CO ₂	6	L	Khoo (1990)
V_{iO_2}	Body tissue storage volume for O ₂	7.7	L	Khoo (1990)
MR_{CO_2}	Metabolic production rate for CO ₂	0.0033	1/s STPD	Khoo (1990)
MR_{O_2}	Metabolic consumption rate for O ₂	0.0038	1/s STPD	Khoo (1990)
C_{vCO_2IC}	Initial condition for mixed venous CO ₂ concentration	0.5247	ml/ml	Khoo (1990)
C_{vO_2IC}	Initial condition for mixed venous O ₂ concentration	0.1639	ml/ml	Khoo (1990)

Table 1 (Continued)

Parameter	Definition	Values	Units	Source
Upper airway model				
R_{uaw}	Upper airway wall resistance	1,000,000	cmH ₂ O s/L	Model
A_{0ua}	Maximum area of opening in upper airway	1	a.u.	Model
K_{ua}	Proportionality coefficient between A_{ua} and Y_{ua}	1	L/(s cmH ₂ O)	Model
$P_{crit,awake}$	Critical upper airway pressure in wakefulness	−40	cmH ₂ O	Model
S_{ua}	Upper airway sensitivity to collapse	0.01	a.u.	Model
C_{ua}	Upper airway compliance	Variable	L/cmH ₂ O	Model
P_{ua}	Upper airway pressure	Variable	cmH ₂ O	Model
\dot{V}_{ua}	Upper airway flow	Variable	cmH ₂ O	Model
\dot{V}	Total flow in airways	Variable	cmH ₂ O	Model
Respiratory muscle activity				
FlowIC	Initial air flow	0	L/s	Model
VC	Vital capacity	5	L	Model
Pt.frclC1	Initial condition for respiratory muscle reaction	0	spikes/s	Model
Pt.frclC2	Initial condition for respiratory muscle reaction	0	spikes/s	Model
FlowIC	Initial condition for airflow	0	L/s	Model
VtIC	Initial condition for lung volume	0	L	Model
Central neural control				
Carotid baroreceptors				
P_n	Center pressure for sigmoidal function	92	mmHg	Ursino (1998)
K_{cs}	Parameter for sigmoidal slope control	11.758	mmHG	Ursino (1998)
$P_{n, sleep}$	Parameter for sleep effects	0	mmHg	Model
$K_{cs, sleep}$	Parameter for sleep effect	0	mmHG	Model
$f_{cs, min}$	Lower threshold for sigmoidal function	2.52	spikes/s	Ursino (1998)
$f_{cs, max}$	Upper saturation for sigmoidal function	47.78	spikes/s	Ursino (1998)
τ_z	Time constant for baroreflex	6.37	s	Ursino (1998)
τ_p	Time constant for baroreflex	2.076	s	Ursino (1998)
Ventilatory response				
I_c	Central apneic threshold	45	Dimensionless	Model
I_{pCO_2}	Peripheral apneic threshold for CO ₂	38	Dimensionless	Model
I_{pO_2}	Peripheral apneic threshold for O ₂	102.4	Dimensionless	Model
G_c	Gain for central chemical drive	0.075	Dimensionless	Model
G_p	Gain for peripheral chemical drive	0.0063	Dimensionless	Model
S_{wake}	Factor of wakefulness to sleep	0.3	Dimensionless	Model
Chemoreflex control of variable respiratory rhythm				
F_b	Basal breathing frequency	12.5	Breath/min	Duffin et al. (2000)
V_b	Basal ventilation	6.7	L/min	Model
T_D	Chemoreflex drive threshold	1539	mL	Duffin et al. (2000)
T_p	Chemoreflex drive threshold	2879	mL	Model
$S1_F$	Scaling factor	0.00518	Dimensionless	Duffin et al. (2000)
$S1_V$	Scaling factor	0.024	Dimensionless	Duffin et al. (2000)
$S2_F$	Scaling factor	0.0105	Dimensionless	Duffin et al. (2000)
$S2_V$	Scaling factor	0.0367	Dimensionless	Duffin et al. (2000)
Chemoreflex				
$f_{chemo, max}$	Upper saturation for the sigmoidal function	12.3	spikes/s	Magosso and Ursino (2001)
$f_{chemo, min}$	Lower saturation for the sigmoidal function	0.835	spikes/s	Magosso and Ursino (2001)
$f_{chemo, control}$	Basal level for the chemoreflex	1.4	Dimensionless	Magosso and Ursino (2001)
K_{chemo}	Slope control parameter for the sigmoidal function	29.27	mmHg	Magosso and Ursino (2001)
K_H	Constant value for the static response	3	Dimensionless	Magosso and Ursino (2001)
τ_{chemo}	Time constant for the chemoreflex	2	s	Magosso and Ursino (2001)
Lung stretch receptors reflex				
G_{ls}	Constant gain	23.29	spikes/s/L	Magosso and Ursino (2001)
τ_{ls}	Time constant	2	s	Magosso and Ursino (2001)
Offsets				
X_{sa}	Saturation for the offset of α -sympathetic activity on peripheral resistance	6	Torr	Magosso and Ursino (2001)
θ_{san}	Nominal level of offset of α -sympathetic activity on peripheral resistance	13.2	spikes/s	Magosso and Ursino (2001)
$P_{O_2, nsa}$	Central point for the sigmoidal function	30	Torr	Magosso and Ursino (2001)
$kisc_{sa}$	Parameter of α -sympathetic activity on peripheral resistance	2	Dimensionless	Magosso and Ursino (2001)
X_{sb}	Saturation for the offset of β -sympathetic activity	21.2	Torr	Model
θ_{sbn}	Nominal level of offset of β -sympathetic activity	3.6	spikes/s	Magosso and Ursino (2001)
$P_{O_2, nsb}$	Central point for the sigmoidal function	45	Torr	Magosso and Ursino (2001)
$kisc_{sb}$	Parameter of β -sympathetic activity	4	Dimensionless	Magosso and Ursino (2001)
X_{sp}	Saturation for the offset of α -sympathetic activity on peripheral resistance	6	Dimensionless	Magosso and Ursino (2001)
θ_{spn}	Nominal level of offset of α -sympathetic activity on peripheral resistance	13.2	spikes/s	Magosso and Ursino (2001)

Table 1 (Continued)

Parameter	Definition	Values	Units	Source
$P_{O_2,ns}$	Central point for the sigmoidal function	30	Torr	Magosso and Ursino (2001)
$k_{isc,sp}$	Parameter of α -sympathetic activity on unstressed volume of veins	2	Dimensionless	Magosso and Ursino (2001)
τ_{isc}	Time constant for oxygen response	30	s	Magosso and Ursino (2001)
τ_{cc}	Time constant for carbon dioxide response	20	s	Magosso and Ursino (2001)
Autonomic control				
$f_{cs,0}$	Center point for the sigmoidal function for parasympathetic	25	spikes/s	Magosso and Ursino (2001)
$f_{para,0}$	Lower saturation of the parasympathetic exponential decay function	3.2	spikes/s	Magosso and Ursino (2001)
$f_{para,\infty}$	Upper limit of the parasympathetic exponential decay function	6.3	spikes/s	Magosso and Ursino (2001)
k_p	Slope control parameter for the sigmoidal function	7.06	Dimensionless	Magosso and Ursino (2001)
$G_{RSA,p}$	Central RSA gain for parasympathetic response	0.4	Dimensionless	Model
$G_{chemo,p}$	Chemoreflex gain for parasympathetic response	0.03	Dimensionless	Model
$G_{lung,p}$	Lung stretch receptor reflex gain for parasympathetic response	0.24	Dimensionless	Magosso and Ursino (2001)
$f_{s,0}$	Upper limit of the sympathetic exponential decay function	16.11	spikes/s	Magosso and Ursino (2001)
$f_{s,\infty}$	Lower saturation of the sympathetic exponential decay function	2.1	spikes/s	Magosso and Ursino (2001)
K_s	Constant for the exponential function	0.07	s	Magosso and Ursino (2001)
$G_{RSA,bs}$	Central RSA gain for β -sympathetic response	0.4	Dimensionless	Model
$G_{chemo,bs}$	Chemoreflex gain for β -sympathetic response	2.8	Dimensionless	Model
$G_{lung,bs}$	Lung stretch receptor reflex gain for β -sympathetic	0.24	Dimensionless	Model
$G_{RSA,as}$	Central RSA gain for α -sympathetic response	0.4	Dimensionless	Model
$G_{chemo,as}$	Chemoreflex gain for α -sympathetic response	4	Dimensionless	Model
$G_{lung,as}$	Lung stretch receptor reflex gain for α -sympathetic	0.34	Dimensionless	Magosso and Ursino (2001)
β-Sympathetic response				
f_{tbsiC}	β -Sympathetic initial output after time delay	3.8576	spikes/s	Ursino (1998)
$f_{tbs,min}$	Lower limit for the natural log function	2.66	spikes/s	Ursino (1998)
G_{bs}	β -Sympathetic Gain varied with sleep drive	-0.13	Dimensionless	Ursino (1998)
$G_{bs,sleep}$	β -Sympathetic sleep gain factor	0.2	Dimensionless	Model
τ_{bs}	β -Sympathetic time constant	2	s	Ursino (1998)
D_{bs}	Delay for β -sympathetic time constant	2	s	Ursino (1998)
Parasympathetic response				
f_{tptC}	Para sympathetic initial output after time delay	4.2748	spikes/s	Ursino (1998)
G_{para}	Parasympathetic Gain varied with sleep drive	0.09	Dimensionless	Ursino (1998)
$G_{para,sleep}$	Parasympathetic sleep gain factor	0.2	Dimensionless	Model
τ_{para}	Parasympathetic time constant	1.5	s	Ursino (1998)
D_{bs}	Delay for parasympathetic time constant	0.2	s	Ursino (1998)
Neuromuscular drive				
Inhale	Boolean variable for inhalation	1	Dimensionless	Model
Sino-atrial node				
HP_{basal}	Basal value for HP for denervated heart	0.58	s	Ursino (1998)
Maximum end-systolic elastance				
G_{lv}	Elastance gain for left ventricle	0.475	mmHg/mL/v	Ursino (1998)
D_{lv}	Delay for elastance of left ventricle	2	s	Ursino (1998)
τ_{lv}	Time constant for elastance of left ventricle	8	s	Ursino (1998)
$Emax0_{lv}$	Basal level of maximum end-systolic elastance of left ventricle	2.392	mmHg/mL	Ursino (1998)
G_{rv}	Elastance gain for right ventricle	0.282	mmHg/mL/v	Ursino (1998)
D_{rv}	Delay for elastance of right ventricle	2	s	Ursino (1998)
τ_{rv}	Time constant for elastance of right ventricle	8	s	Ursino (1998)
$Emax0_{rv}$	Basal level of maximum end-systolic elastance of right ventricle	1.412	mmHg/mL	Ursino (1998)
α-Sympathetic control of peripheral resistance				
f_{asiC}	α -Sympathetic initial output after time delay	34.793	spikes/s	Ursino (1998)
$f_{as,min}$	Lower limit for the natural log function	2.66	spikes/s	Ursino (1998)
$G_{as,sleep}$	α -Sympathetic gain varied with sleep	0.3	Dimensionless	Model
$G_{as,sp}$	α -Sympathetic gain for splanchnic peripheral resistance	0.695	Dimensionless	Ursino (1998)
$\tau_{as,sp}$	α -Sympathetic time constant	2	s	Model
$D_{as,sp}$	Delay α -sympathetic time constant	2	s	Ursino (1998)
$G_{as,ep}$	α -Sympathetic gain for extrasplanchnic peripheral resistance	1.94	Dimensionless	Ursino (1998)
$\tau_{as,ep}$	α -Sympathetic time constant	2	s	Ursino (1998)
$D_{as,ep}$	Delay α -sympathetic time constant	2	s	Ursino (1998)
$G_{as,mp}$	α -Sympathetic gain for skeletal muscle peripheral resistance	2.47	Dimensionless	Ursino (1998)

Table 1 (Continued)

Parameter	Definition	Values	Units	Source
$\tau_{as.mp}$	α -Sympathetic time constant	2	s	Model
$D_{as.mp}$	Delay α -sympathetic time constant	2	s	Ursino (1998)
V_{usv0}	Basal level of unstressed volume of splanchnic venous circulation	1435.4	mL	Ursino (1998)
$G_{as.usv}$	α -Sympathetic gain for unstressed volume of splanchnic venous circulation	-265.4	mL/v	Ursino (1998)
$\tau_{as.usv}$	α -Sympathetic time constant	20	s	Ursino (1998)
$D_{as.usv}$	Delay α -sympathetic time constant	5	s	Ursino (1998)
Local blood flow control of peripheral resistance				
$P_{aCO_2.n}$	Nominal arterial CO ₂ partial pressure i	40	Torr	Magosso and Ursino (2001)
$CvO_2.n.b$	Nominal venous O ₂ concentration in cerebral peripheral circulation	0.14	Dimensionless	Magosso and Ursino (2001)
$CvO_2.n.m$	Nominal venous O ₂ concentration in skeletal muscle peripheral circulation	0.155	Dimensionless	Magosso and Ursino (2001)
$CvO_2.n.h$	Nominal venous O ₂ concentration in coronary peripheral circulation	0.11	Dimensionless	Magosso and Ursino (2001)
$\tau_{au.CO_2}$	Time constant for peripheral CO ₂ response	20	s	Magosso and Ursino (2001)
$\tau_{au.O_2}$	Time constant for peripheral O ₂ response	10	s	Magosso and Ursino (2001)
A	Parameter for flow regulation equation	20.9	Dimensionless	Magosso and Ursino (2001)
B	Parameter for flow regulation equation	92.8	Dimensionless	Magosso and Ursino (2001)
C	Parameter for flow regulation equation	10,570	Dimensionless	Magosso and Ursino (2001)
$G_{O_2.b}$	Gain of local O ₂ response on cerebral vascular bed	10	Dimensionless	Magosso and Ursino (2001)
$G_{O_2.h}$	Gain of local O ₂ response on coronary vascular bed	35	Dimensionless	Magosso and Ursino (2001)
$G_{O_2.m}$	Gain of local O ₂ response on muscular vascular bed	30	Dimensionless	Magosso and Ursino (2001)
Sleep mechanism				
A	Amplitude of the skewed sine function	20.9	Dimensionless	Model
X_H	Bias of the skewed sine function for process CH	0.9	Dimensionless	Model
X_L	Bias of the skewed sine function for process CL	0.15	Dimensionless	Model
α_{gc}	Constant for sleep decaying	0.2/60	Dimensionless	Model
α_{rc}	Rising rate of slow-wave activity	0.4/60	Dimensionless	Model
α_{fc}	Falling rate of slow-wave activity	0.008/60	Dimensionless	Model
SWAo	Initial value of sleep-wake activity	0.007	Dimensionless	Model

signal, analogous to the R–R interval. IPFM has been used in previous simulation studies for this purpose (Dempsey et al., 2002). The vagal effect on heart rate is modeled assuming first-order dynamics with the sleep index modulating the gain. Beta-sympathetic activity is assumed to affect heart rate along with ventricular contractility through a gain that is also modulated by the sleep index. The effect on ventricular contractility takes the form of a time-varying nonlinear elastance function that modulates systolic period and thus cardiac output. The diastolic filling time, the difference between the heart period and systolic period, is thus controlled indirectly. The activation of the right and left hearts is assumed to be fully synchronized and to occur simultaneously. Stroke volume can vary under the influence of venous return, heart period and contractility, and circulatory blood flows in pulmonary and systemic circulation systems are determined by the stroke volume and peripheral vascular tone.

Alpha-sympathetic activity controls the main part of the total peripheral resistance (TPR) change in terms of peripheral vascular tone, as characterized by the changes in peripheral resistances and unstressed volumes of blood vessels in splanchnic, extrasplanchnic and muscular peripheral circulations. Local blood flow in the peripheral vasculature is mediated by changes in the resistances of muscular, coronary and cerebral peripheral circulations, as determined by the local P_{O_2} and P_{CO_2} of the blood in these vascular beds. The changes in these local resistances contribute to the overall TPR change. The carotid sinus perceives the changes of arterial blood pressure and converts them into nerve activities for autonomic control, considered as baroreflex autonomic input.

The model of autonomic control assumes that the autonomic inputs that affect the cardiovascular system include the efferent neural outputs of the baroreceptors, chemoreceptors and pulmonary stretch receptors, and CNS response to arterial P_{CO_2} and P_{O_2} .

These inputs are integrated to produce autonomic outputs independently, including beta-sympathetic activity and parasympathetic efferent activity to the heart, and alpha-sympathetic activity to the peripheral vasculature. For sympathetic activities, the efferent firing rates are exponential functions of the weighted sum of the afferent activities and offsets. This section of the model allows the simulation of respiratory to cardiovascular effects such as respiratory sinus arrhythmia, pleural pressure modulation of pulmonary circulatory pressures and blood flow, and chemoreflex effects on peripheral vascular resistance. The cardiovascular changes in turn affect respiratory control through changes in gas exchange dynamics and circulatory delays resulting from changes in blood flow. The CNS response to arterial P_{O_2} and P_{CO_2} in the cerebral blood flow provides outputs of the offset terms for alpha-sympathetic activity corresponding to peripheral resistance change and vein constriction and offsets for beta-sympathetic activity with respect to heart rate modulation, based on the work of Magosso and Ursino (2001).

2.3. Sleep mechanism (Appendix Eqs. (A.74)–(A.83))

The sleep mechanism is a two process model from the Borbely group (Achermann and Borbely, 2003; Borbely and Achermann, 2000; Daan et al., 1984). The total sleep propensity is determined by the combination of two processes: a sleep independent circadian process C and a sleep dependent slow-wave process S. The process C sets up a high and a low time-variant circadian threshold C_H and C_L to modulate the sleep indication, respectively. The circadian process C is described using a skewed sine function which provides the normal 16 h of wake state and 8 h of sleep period. The process S is oscillating between these two thresholds, and when it raises upon or beyond the high one, the sleep is triggered; when it falls on or below the low one, the sleep is terminated and awaked

activity starts. The sleep–wake activity (SWA) wave represents the stage of sleep and it is regulated by both process S and C and non-rapid eye movement (NREM) sleep and rapid eye movement (REM) sleep with a falling and a rising factors, respectively. By varying the interval between those two thresholds, the duration of sleep is manipulated and automatically different night by night. Because of this flexibility, not only can the model simulate regular sleep patterns, it can also evaluate abnormal cases such as the effects of sleep deprivation. The time-course of process S is chosen based on experimental data on recordings of slow-wave sleep. The time-course for process S activity during awake is described from the interpolation of experimental data points which show an exponential increase with saturation.

The sleep mechanism model affects the respiratory and cardiovascular subsystems mainly through the sleep state index, SI, which provides an indication of whether the model is “awake” (SI=0) or “asleep” (SI=1). During sleep onset, SI is a scaled version of SWA as S_{SWA} , following the same time-course and attaining the value of unity (“asleep”) when SWA reaches its first and highest maximum value. The NREM and REM stages during sleep are simulated through a pulse train and are represented by changes in SWA with no activity in REM stage and an overall tendency to decay throughout the night during NREM sleep.

In the case of obstructive sleep apnoea, during the upper airway obstruction, arterial P_{CO_2} increases as arterial P_{O_2} and S_{aO_2} decrease, allowing the resulting chemical drive to progressively rise. When the total ventilatory drive exceeds the arousal threshold, arousal is triggered and the upper airway opens up allowing the resumption of airflow. The arousal threshold is assumed to be linearly related to S_{SWA} : the threshold is higher when S_{SWA} is higher and close to 1 during NREM sleep and it is lower when S_{SWA} is close to zero during REM sleep (see Eq. (A.80)). This assumption is based on empirical data showing that the threshold for arousal is lower, during REM stage than in NREM stage (Berry et al., 1998; Berry and Gleeson, 1997; Khoo et al., 1996a,b). During arousal, the wakefulness stimulus reappears, but as ventilatory drive drops back below the threshold, the wakefulness stimulus disappears once again as the system reverts to its previous level of sleep propensity.

2.4. Software implementation

PNEUMA is implemented using SIMULINK®, which provides a powerful high level visually-oriented environment for modeling, simulating, and analyzing dynamic systems. The model contains 472 parameters and 80 states, and allows graphical access to 113 variables. It takes approximately 114 min to run a 48 h simulation and about 60 h to run a 10-week simulation on a PC with Intel Core 2 Duo E8500 CPU. PNEUMA is a hybrid model that contains both discrete and continuous modes of implementation, allowing it to simulate dynamic behavior over a time scale that ranges from milliseconds to days (i.e. intra-heart beat events to circadian rhythms). An accompanying graphical user interface panel allows users to conveniently change the values of a large number of parameters or impose a variety of physiological conditions without having to modify the program directly. Advanced users can vary parameter values or make changes to the underlying models by directly modifying the graphical objects in the SIMULINK® code.

2.5. Model parameters and verification issues

Wherever possible, the parameter values employed in the model are based on population values published in the literature, as indicated in Table 1. In some cases where the physiological values are unclear, the parameters have been tuned to ensure that the dynamic behavior of the model under the various conditions explored remains realistic. Model verification and validation are

performed by comparing the simulation output under baseline conditions in normal breathing and sleep-disordered breathing and under different interventions to the general population-averaged cardiorespiratory data reported in the literature. Since the focus of this study is on the dynamic interactions among the various mechanisms at play in cardiorespiratory control, verification and validation are guided by employing a qualitative goodness of fit approach. This contrasts with smaller, more focused models in which the key parameters are estimated based on quantitative fits to experimental data obtained from individual subjects. In the present case, there is no single complete experimental dataset that the model can be validated against. Rather, we focus on comparing the model responses with the empirically derived responses that represent the “average subject” in each patient/subject population. The utility of this comprehensive, highly parameterized model is “proven” by testing the internal consistency of the simulated responses of a significant number of state variables over a range of perturbations and conditions.

3. Results: model simulations

3.1. Simulation of cardiorespiratory control during sleep onset in normals

Normal sleep onset is generally associated with a reduction in sympathetic activity and increase in parasympathetic tone, leading to a fall in heart rate and reductions in systolic and diastolic blood pressures, along with an accompanying decrease in ventilation (Mancia, 1980). Subsequently, there are ultradian fluctuations in autonomic activity controlling coronary artery tone (Kirby and Verrier, 1989; Verrier and Dickerson, 1991), systemic blood pressure (Dempsey et al., 2002) and heart rate (Baust and Bohnert, 1969; Mancia, 1980). The transition from wakefulness to sleep in normal breathing as predicted by the model is shown in Fig. 2. There is a reduction in total ventilatory drive due to the withdrawal of the wakefulness stimulus and a decrease in chemoreflex gain. Thus, ventilation drops, resulting in a small increase in P_{aCO_2} and slight decrease in S_{aO_2} which allows the respiratory system to compensate partially for the initial sleep state-related drop in ventilation. As such, both tidal volume and respiratory frequency first exhibit a small undershoot before settling at levels lower than during wakefulness. In the normal subject, the increase in parasympathetic tone and decrease in sympathetic tone results in the lower heart rate (higher heart period) and lower arterial blood pressure.

3.2. Valsalva maneuver

In the Valsalva maneuver, a subject performs a forced expiration against an occluded airway after a deep inspiration. The Valsalva maneuver is frequently employed as a test of autonomic cardiovascular function (Bannister, 1980; Fox et al., 1966). The maneuver markedly elevates intrathoracic pressure, thus affecting venous return, myocardial contractility, vasomotor tone and baroreflex heart rate control (Fox et al., 1966). The hemodynamic response to the Valsalva maneuver has four distinct phases (Bannister, 1980). At the beginning of forced expiration (phase 1), the contraction of thoracic cage compresses the lungs and causes a large rise in pleural pressure (P_{pl}). This intrathoracic pressure compresses the blood vessels within the chest. Aortic compression results in a transient increase in arterial blood pressure (ABP), which produces a brief bradycardia (heart rate decrease). Because the thoracic vena cava also becomes compressed, venous return to the heart is decreased, resulting decrease in cardiac output. This leads to an increased tachycardia (heart rate increase) for the 10 s of sustained forced expiration (phase 2) and a fall in ABP. But the decrease in ABP

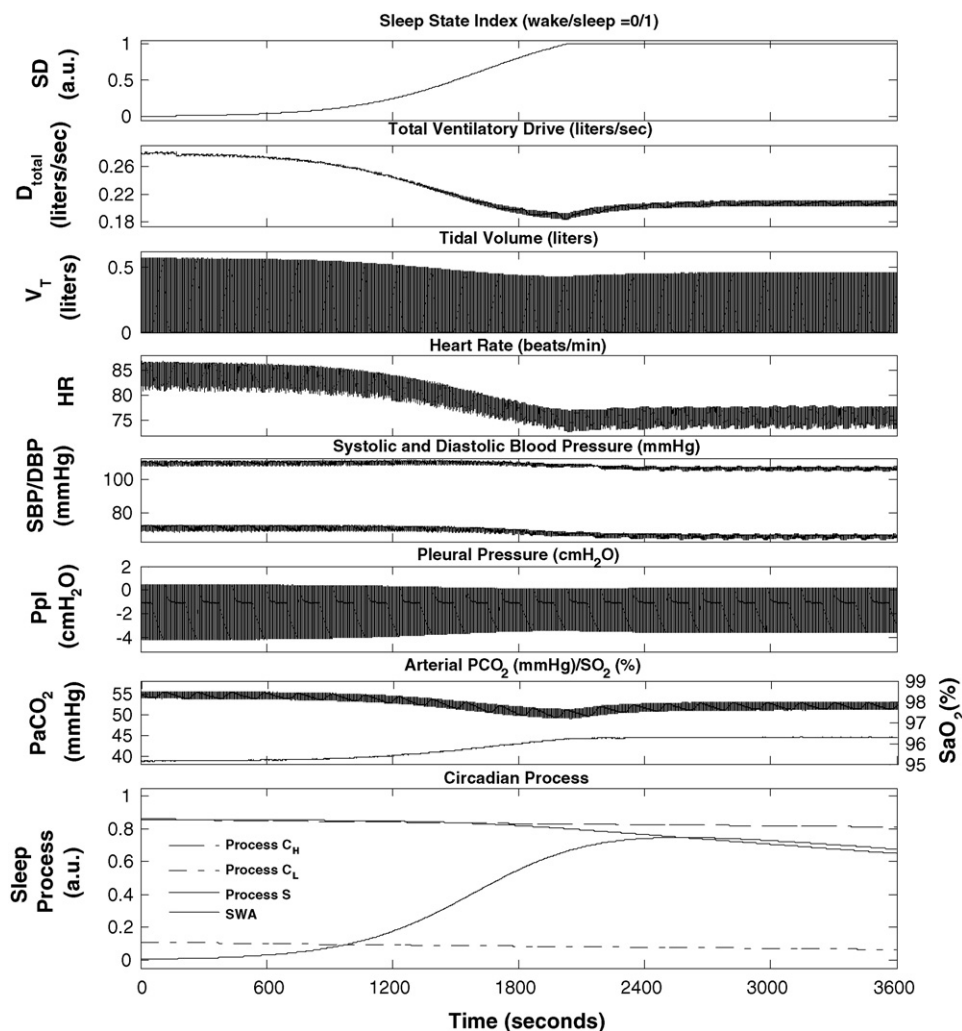


Fig. 2. Simulation of wakefulness to sleep transition in a normal subject.

ceases after a few seconds if the peripheral sympathetic vasoconstriction response is normal. Once the occlusion is released (phase 3), the immediate drop in P_{pl} induces a decrease in ABP. The heart rate remains high due to the increased sympathetic tone. In phase 4, the delayed sympathetic response leads to an ABP overshoot and a compensatory bradycardia. Fig. 3B displays the results of a model simulation of the effects of the Valsalva maneuver on respiration, ABP and heart rate. The forced expiration against closed airway starts at $t=84$ s and ends at $t=98$ s. The simulated results for phase 1 through 4 are as indicated on Fig. 3B. Comparison with published experimental data from Bannister (1980) displayed in Fig. 3A, shows good agreement. Although the results are not shown here, the model is able to also realistically simulate the effects of the Mueller maneuver – some of these effects involve the same mechanisms that dominate during obstructive apnoea (see Section 3.4).

3.3. Effects of changes in chemoreflex stimulation

The model assumes that hypercapnia stimulates both central and peripheral chemoreceptors while hypoxia affects only the peripheral chemoreceptors (Cooper et al., 2005; Spicuzza et al., 2005). Central depression by hypoxia has not been included in this model. Central chemoreceptor stimulation leads to increased ventilation as well as increased sympathetic outflow – the latter produces peripheral vasoconstriction, increased cardiac contractility and heart rate acceleration (Magosso and Ursino, 2001). Carotid

chemoreceptor stimulation also produces peripheral vasoconstriction via the sympathetic pathways, but at the same time, there is an increased cardiac vagal activity leading to a slowing of heart rate (Ursino and Magosso, 2003). However, there is a significant degree of both competitive and reinforcing interaction among these different factors. For instance, during hypoxia, the increased ventilation acts via the lung stretch receptors to inhibit vagal outflow to the heart, while both the peripheral chemoreflex and the baroreflex act to increase cardiac vagal activity. Whether the net result is tachycardia or bradycardia depends on which of these competing effects dominate. The effect of hypoxia on sympathetic activity also consists of excitatory influence from the peripheral chemoreceptors balanced by the inhibitory influence of the lung stretch receptors (Somers et al., 1989a,b). All these features have been incorporated into the model.

Fig. 4 illustrates the behavior of the model when the inhaled level of O_2 concentration is lowered from 21% to 10% to induce hypoxia, but the P_{aCO_2} level is dynamically maintained around its normal level of ~ 38.8 mmHg by increasing inspired P_{CO_2} accordingly. The simulation shows a transient period of ~ 1 min immediately following the induction of hypoxia before P_{aCO_2} is restored to a stable level. The hypoxia simulation begins at $t=800$ s and lasts for 300 s. Accompanying the increased ventilatory drive and ventilation, are parallel increases in heart rate and ABP. ABP is now displayed in terms of beat-to-beat systolic (SBP) and diastolic (DBP) pressures. Note that respiratory sinus arrhythmia also

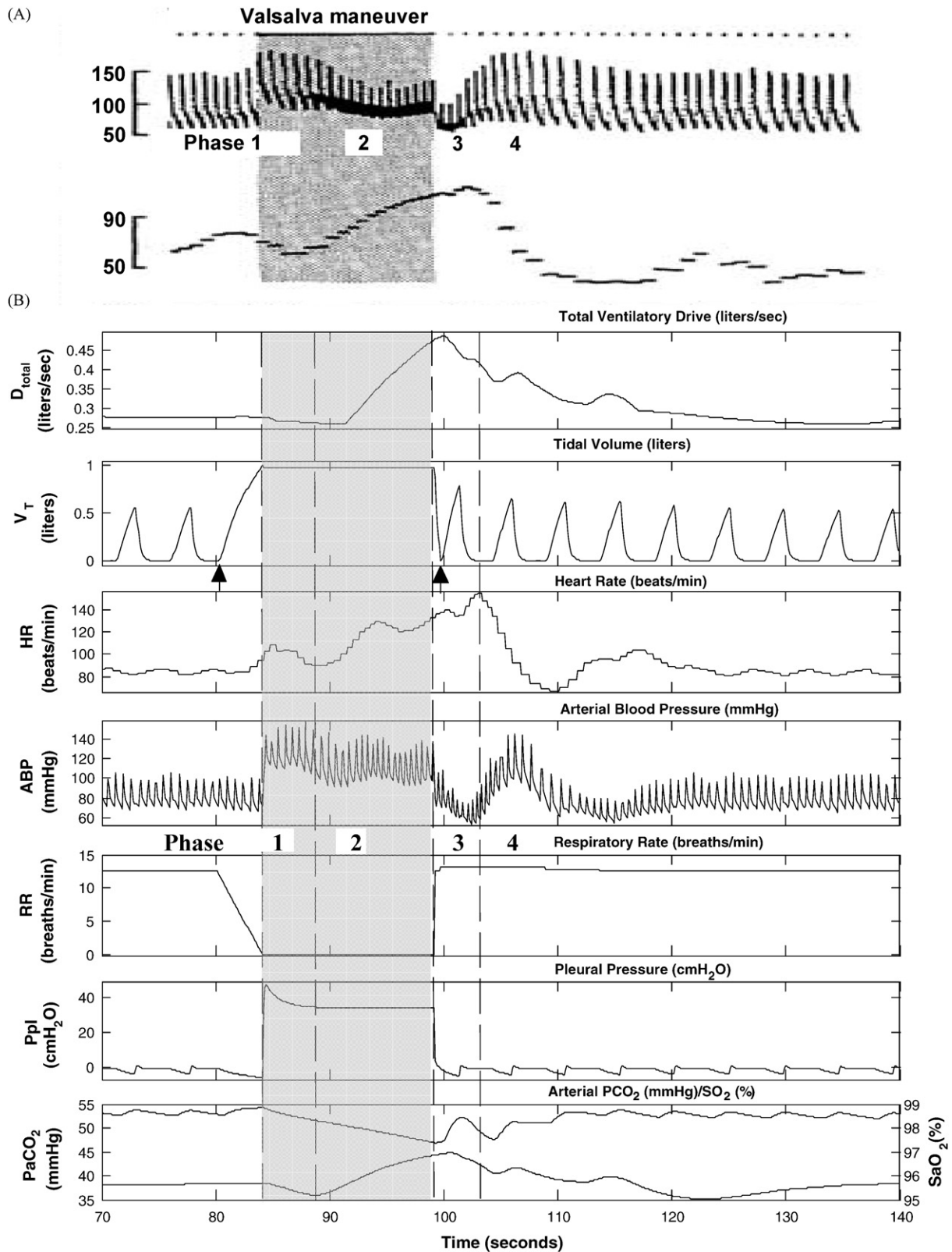


Fig. 3. Valsalva maneuver. (A) Experimental data from Bannister (4). (B) Model results. The maneuver begins at time 80s with a deep inspiration and ends at ~100s with release of the breathhold (indicated by arrows).

increases because of the larger tidal volumes in the breathing pattern. These model predictions are consistent with reported experimental findings (Magosso and Ursino, 2001; Narkiewicz et al., 1999; Somers et al., 1989a,b).

Fig. 5 summarizes the steady state responses of the major cardiorespiratory variables in the model to the various combinations of hypoxia with hypocapnia, normocapnia or hypercapnia, induced through simulated inhalation of 8.5% O₂ along with 0% (hypocap-

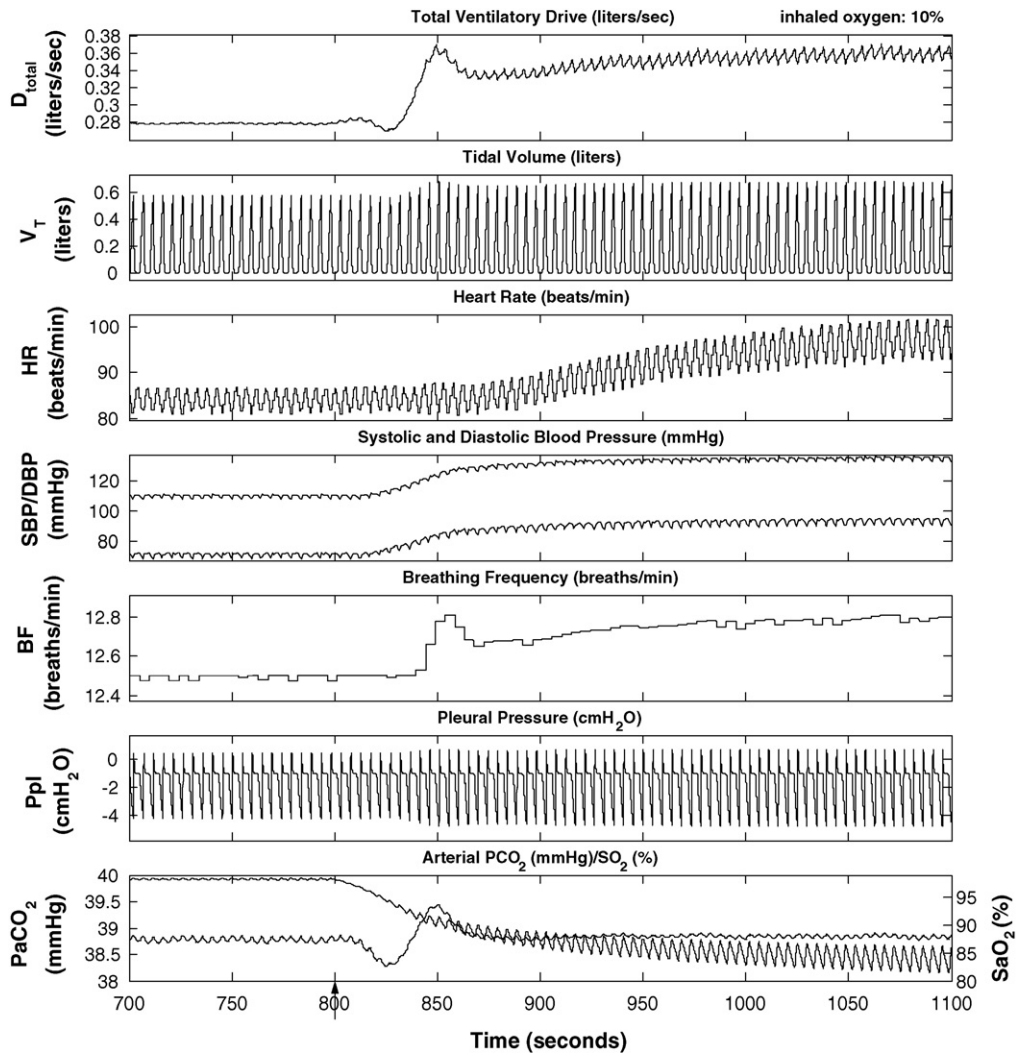


Fig. 4. Simulation of isocapnic hypoxia. Inhaled oxygen is changed from 21% to 10%, starting at 800 s (arrow).

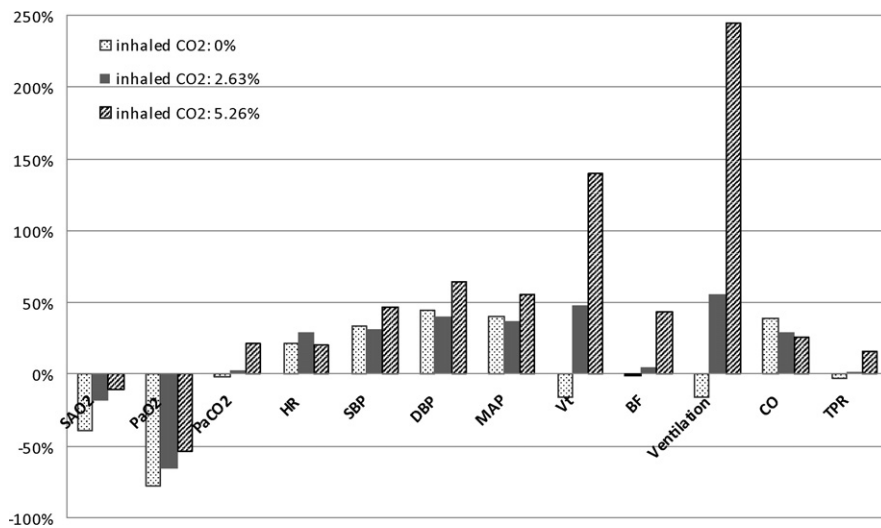


Fig. 5. Steady state cardiorespiratory responses of the model to various combinations of hypoxia (inhaled O₂ = 8.5%) with hypocapnia (inhaled CO₂ = 0%), normocapnia (inhaled CO₂ = 2.63%) and hypercapnia (inhaled CO₂ = 5.26%), displayed in terms of percent change from the baseline in normoxic normocapnia. S_{aO₂}: arterial blood oxygen saturation; P_{aO₂}: partial pressure of oxygen in arterial blood; P_{aCO₂}: partial pressure of carbon dioxide in arterial blood; HR: heart rate; SBP: systolic blood pressure; DBP: diastolic blood pressure; MAP: mean arterial blood pressure; V_t: tidal volume; BF: breathing frequency; CO: cardiac output; TPR: total peripheral resistance of all peripheral vasculature in the systemic circulation.

nia), 2.63% CO₂ (normocapnia) and 5.26% CO₂ (hypercapnia). These results are displayed as percent changes of each variable from its baseline control value (air inhalation). As might be expected, P_{aCO_2} and ventilation increase progressively from hypocapnic to isocapnic to hypercapnic hypoxia, while the reductions in mean S_{aO_2} and P_{aO_2} become progressively smaller. In hypocapnia hypoxia, total peripheral resistance (TPR) actually decreases slightly due to the local vasodilatory effect of hypoxia at the capillary level, but nevertheless, SBP and DBP increase because of the increases in heart rate (HR) and stroke volume. As P_{aCO_2} is increased with progressively higher levels of inhaled CO₂, TPR increases as sympathetic drive is increased, leading to increased blood pressure and lower cardiac output. These results from our simulations are consistent with what has been published in the literature (Koehler et al., 1980; Kontos et al., 1967; Magosso and Ursino, 2001).

3.4. Obstructive sleep apnoea

Obstructive apnoeas during sleep elicit a series of mechanical, hemodynamic, chemical and neural responses (Bradley and Floras, 2003a). The inspiratory efforts against the occluded pharynx lead to abrupt reductions in intrathoracic pressure. While sympathetic nervous system activity is normally reduced in sleep (Dempsey et al., 2002; Lanfranchi and Somers, 2001), during apnoea, the inhibitory vagal input from the pulmonary stretch receptors that restrains sympathetic activities during normal breathing is reduced. This leads to a considerably higher level of central sympathetic outflow during obstructive apnoea. The consequent hypercapnic hypoxia further increases chemoreflex-induced sympathetic discharge, while the resulting vasoconstriction from increased alpha-sympathetic activity elevates peripheral resistance and blood pressure. However, arousal from sleep is triggered when the progressively increasing ventilatory effort resulting from the buildup in chemical drive during apnoea exceeds the arousal threshold – this results in a resumption of airflow through the stimulation of pharyngeal dilator muscle activity which restores airway patency. But the accompanying excitatory input from the chemoreflexes causes a further burst of sympathetic outflow along with a loss of vagal tone (Horner et al., 1995; Somers et al., 1995). As such, arousals are characterized by an intense surge in heart rate and increase in blood pressure (Lanfranchi and Somers, 2001; Leung and Bradley, 2001). The hyperventilatory breaths that accompany arousal rapidly restore blood gases towards normal levels and as the effects of the transient arousal wear off and the system falls quickly back to sleep, allowing the pharynx to be once again susceptible to collapse. In severe OSAS, these cycles of apnoea and arousal can recur several hundred times each night, exposing the cardiovascular system to high amplitude oscillations in heart rate and blood pressure.

To enable the model to simulate OSAS following sleep onset, the upper airway sensitivity parameter (S_{ua}) is increased to a value of at least 0.38 from its control level of 0.01. Several obstructive apnoea episodes are displayed on Fig. 6. Each episode of obstructive apnoea leads to hypoxia and hypercapnia, which generate progressively larger respiratory efforts, as reflected in the augmented pleural pressure fluctuations. Eventually, these ventilatory efforts become large enough to trigger an arousal. The arousal brings with it a surge in sympathetic activity and withdrawal of parasympathetic activity, thus leading to significant increases in heart rate and blood pressure. As upper airway patency and airflow to the lungs are restored, there is a rapid resumption of sleep. Subsequent reductions in the state-related ventilatory drive lead to loss of upper airway patency again and a new cycle of obstructive apnoea followed by arousal begins. The model predicts periodicities on the order of ~52 s, which is consistent with what has been reported in the literature (Lanfranchi and Somers, 2001; Leung and Bradley, 2001).

Fig. 7 displays, on a more extended time scale, the initiation and development of repetitive obstructive apnoea episodes following sleep onset, as predicted by the model. At ~2700 s (0.75 h) into the simulation, continuous positive airway pressure (CPAP) at a level of 15 cmH₂O is applied. Acute abolition of the obstructive apnoea episodes by CPAP prevents recurrent hypoxia, reducing the large swings in heart rate and blood pressure that accompany the alternating periods of upper airway obstruction and arousal. However, once CPAP treatment is terminated the obstructive apnoea episodes resume. Note the increase in mean SBP and DBP following the start of occurrence of the obstructive apnoea episodes, but this elevation of blood pressure is reversed once CPAP is administered. This is consistent with what is known about patients with OSAS being “non-dippers” as opposed to normal “dippers” (Lanfranchi and Somers, 2001; Leung and Bradley, 2001).

Fig. 8 shows the development of repetitive obstructive apnoea episodes in two simulated subjects with OSA: one with normal chemoreflex gain and the other with peripheral chemoreflex gain increased six-fold. The case with normal chemoreflex gain (left panels) displays obstructive hypopnoeas that eventually become obstructive apnoeas. Cycle durations are on the order of 58 s. In the case with elevated peripheral gain (right panels), a combination of central apnoea and obstructive hypopnoea alternating with hyperpnoeas during arousal occurs. The periodicity of these oscillations is substantially shorter, being on the order of 37 s. The main purpose of these simulations is to demonstrate the capability of the model in generating OSA characteristics that range from purely obstructive apnoeas and hypopnoeas to mixed apnoeas with significant durations of central apnoea.

3.5. Hypoxia-induced periodic breathing during sleep

Although periodic breathing (PB) can be induced in awake subjects through hypoxic gas administration or during altitude acclimatization, the tendency to develop PB is enhanced during sleep due to increased hypoxic, hypocapnic and hypercapnic sensitivities (Berssenbrugge et al., 1983). As displayed in Fig. 9, inducing hypoxia by reducing inhaled O₂ concentration from 21% to 10% in during sleep leads to PB. Induced periodic breathing does not occur immediately following hypoxic gas administration but starts to occur only after ~300 s of exposure to hypoxia. Accompanying arousals occur after ~800 s of hypoxic gas administration. Consistent with previous observations (Berssenbrugge et al., 1983; Khoo et al., 1996a, b), full-fledged periodic breathing occurs following a duration over which initially small oscillations in ventilation become progressively amplified. After another 300 s, the model demonstrates stable periodic breathing oscillations. Fig. 9 shows an expanded view of this period of time. It should be noted that the periodicity of the ventilatory oscillation is on the order of 23 s. As well, arousals do not appear at every cycle of PB but only after several PB cycles. Each arousal, when it does appear, tends to occur when ventilatory drive is at its peak. The model also demonstrates hypoxia-induced PB in awake although the results are not shown here. And these results are in good agreement with the literature (Berssenbrugge et al., 1983; Khoo et al., 1991, 1996a,b; Lorenzi-Filho et al., 1999a,b).

3.6. Cheyne–Stokes respiration in chronic heart failure: central sleep apnoea

Cheyne–Stokes respiration (CSR) is characterized by rhythmic oscillations of tidal volume, forming the periodic breathing pattern in which apnoeas and hypopnoeas alternate. CSR with central sleep apnoea (CSA) is common among patients with chronic heart failure (CHF) (Andreas et al., 1996; Bradley and Floras, 2003b). CSR-CSA and OSA have common pathophysiological features including

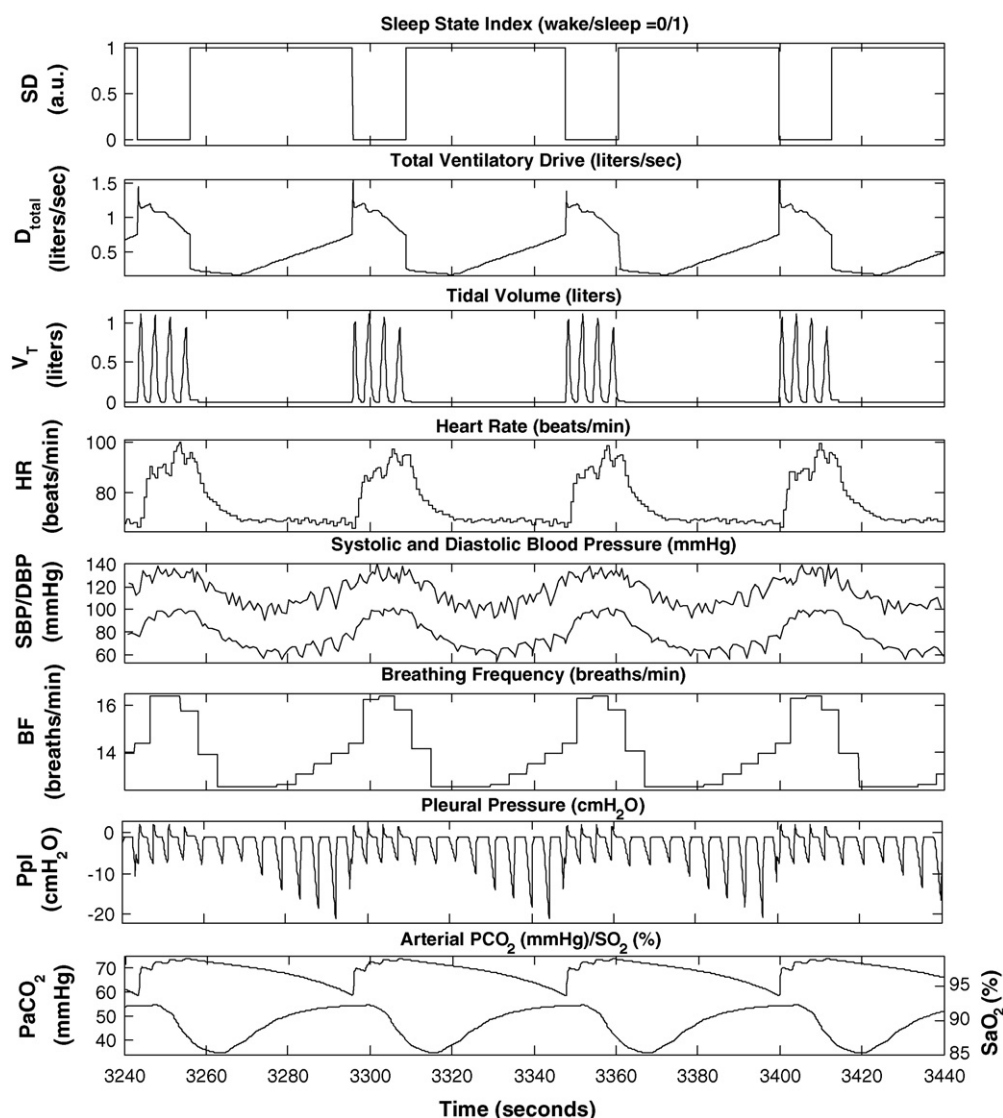


Fig. 6. Simulation of obstructive sleep apnoea.

episodic hypercapnia and arousals from sleep (Leung et al., 2005). However, unlike OSA, no exaggerated negative intrathoracic pressure is presented in CSR-CSA. The cumulative evidence indicates that Cheyne–Stokes respiration with central sleep apnoea is a part of the pathophysiological cycle involving the cardiovascular, pulmonary and autonomic nervous system that contributes to the progression of CHF (Bradley and Floras, 2003b; Ponikowski et al., 1999).

CSR-CSA provokes oscillations in heart rate and blood pressure similar to those seen during OSA: peaks occur during hyperpnoea and valleys occur during apnoea. However, increases in heart rate and blood pressure progress to peak levels more gradually, paralleling the less abrupt increases in ventilation. A necessary factor that contributes to the occurrence of CSR-CSA in patients with severe CHF is the reduced cardiac output which results in prolongation of the circulatory delay between the pulmonary capillaries and the central and peripheral chemoreceptors (Khoo et al., 1991; Leung et al., 2005). However, this factor appears to be insufficient to produce CSR-CSA, since not all patients with CHF exhibit CSR-CSA. As a recent modeling study suggests (Topor et al., 2007), the additional factor of elevated peripheral or central chemoreflex gain appears to be necessary for CSR-CSA to occur. This is supported

by experimental studies that have found that CHF subjects who exhibit CSR-CSA also tend to have higher ventilatory responses to hypercapnia (Javaheri, 1999; Wilcox et al., 1998).

Fig. 10 displays a detailed view of several episodes of CSR-CSA simulated by the model. In this case, peripheral chemoreflex gain was increased six-fold, the effective lung to chemoreceptor vascular volume was increased 1.5 times and cardiac output was decreased by 42% from normal levels by reducing the contractility of the left ventricle. Following sleep onset, the ventilatory drive starts to oscillate visibly and central apnoeas start to appear, creating the PB pattern associated with CSR. CSR-CSA can also be simulated with smaller reductions in cardiac output if peripheral chemoreflex gain is simultaneously increased more. This is consistent with the notion that PB is a manifestation of feedback instability in respiratory control: CSR-CSA can be produced by a combination of two or more of the following factors – increased system delay, increased controller gain, and increased plant gain (Khoo et al., 1991; Topor et al., 2007). The model predicts that the cycle duration of the PB pattern is approximately 60s; this is consistent with the literature. It should be noted that not every hyperpnoeic phase of the CSR-CSA cycle is associated with an arousal.

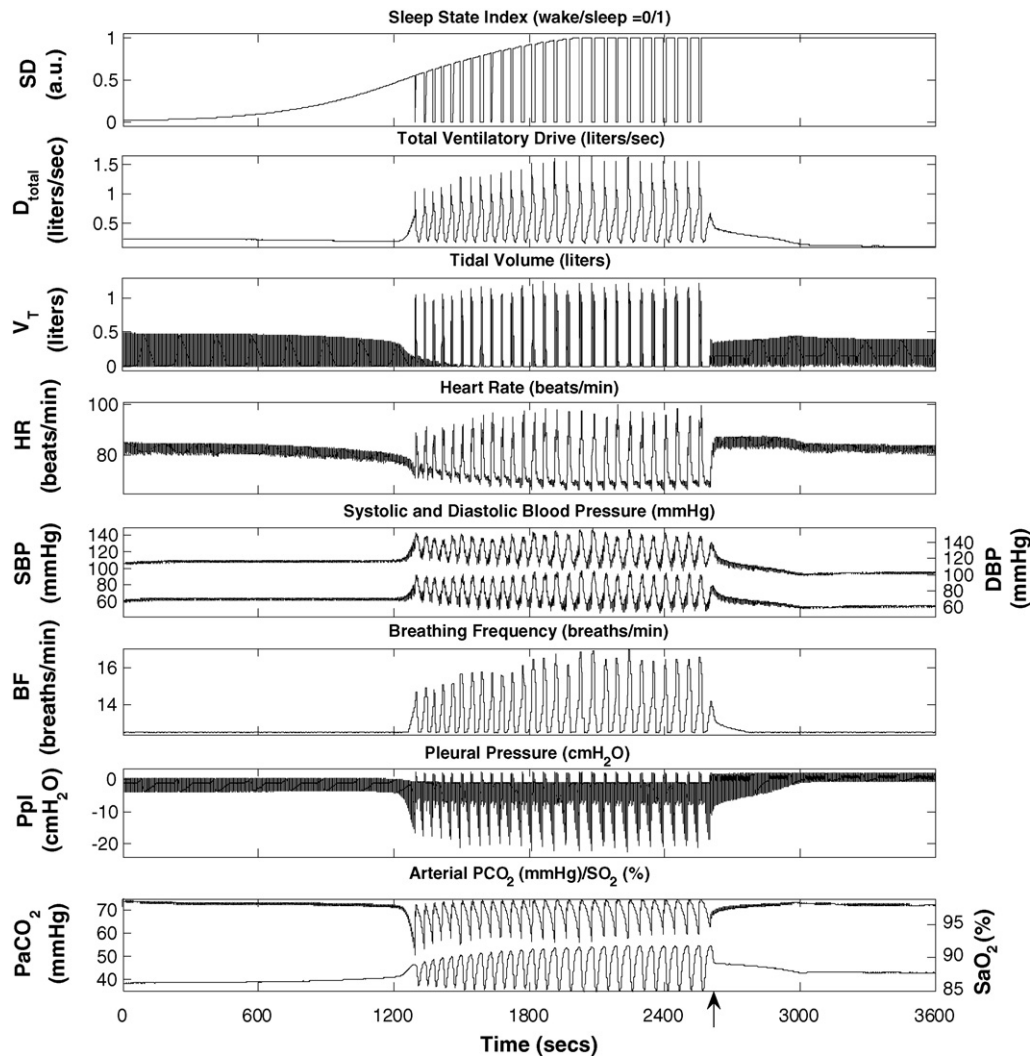


Fig. 7. Simulation showing the development of obstructive sleep apnoea following sleep onset and the effect of subsequent CPAP administration (15 cmH₂O), starting ~0.75 h following the start of the simulation (as indicated by the arrow). Time 0 represents 100 s since the start of the simulation.

Two commonly employed forms of treatment for CSR-CSA are the nocturnal administration of low concentrations of inhaled CO₂ or supplemental O₂. Fig. 11 displays simulations of the effects of CO₂ inhalation and O₂ supplementation on CSR-CSA during sleep. When the inhalation is changed from air to 3.5% CO₂, there is a rapid and complete disappearance of apnoea episodes and periodic breathing, followed by restoration of a stable sleep. In the case of administration of a hyperoxic mixture containing 30% O₂, the model also predicts the complete disappearance of apnoea episodes (slower than CO₂ administration) and marked attenuation of CSR. However, unlike the case with CO₂ administration, PB with hypopnoeas but without accompanying arousals still persists; these simulated characteristics are consistent with empirical data (Lorenzi-Filho et al., 1999a,b).

3.7. Simulation of overnight sleep – normal control vs. obstructive sleep apnoea

In the Borbely model of sleep–wake regulation that we have employed, the sleep propensity index, “Process S”, diminishes as sleep progresses. This continues until $S(t)$ hits the lower circadian threshold C_L of Process C, which represents the circadian rhythm, following which wakefulness appears and $S(t)$ reverses course and starts to increase again (Panel B, Fig. 12). In normal sleep, this model

results in total sleep duration of 7.8 h (Panel A, Fig. 12). However, during OSA or CSR-CSA, the occurrence of repetitive arousals fragments sleep, prolonging the decay of $S(t)$. As a consequence, our model predicts that the overall duration of sleep is about 8.5 h when it is used to simulate an OSA subject (Panels C and D, Fig. 12), and about 8.3 h in a CHF subject with CSR-CSA (not displayed). These total sleep durations for sleep apnoeas are noticeably longer compared to the 7.8 h predicted for normal sleep. However, the overnight administration of CPAP in OSA restores sleep duration back towards the normal duration at ~7.9 h (Fig. 12, Panels E and F). These predictions imply that if the subject with OSA is awakened before sleep propensity is reduced to the levels that normally accompany the end of overnight sleep and the start of wakefulness, there will be a tendency for sleep propensity in the next 24 h to have a higher average value than the previous 24 h. Thus, the model predicts that sleep fragmentation resulting from repetitive arousal in OSA or CSR-CSA would lead to increased daytime sleepiness the following day.

4. Discussion

To date, much has been learnt about the mechanisms that underlie sleep-disordered breathing, as well as the physiological bases through which autonomic cardiovascular control is affected

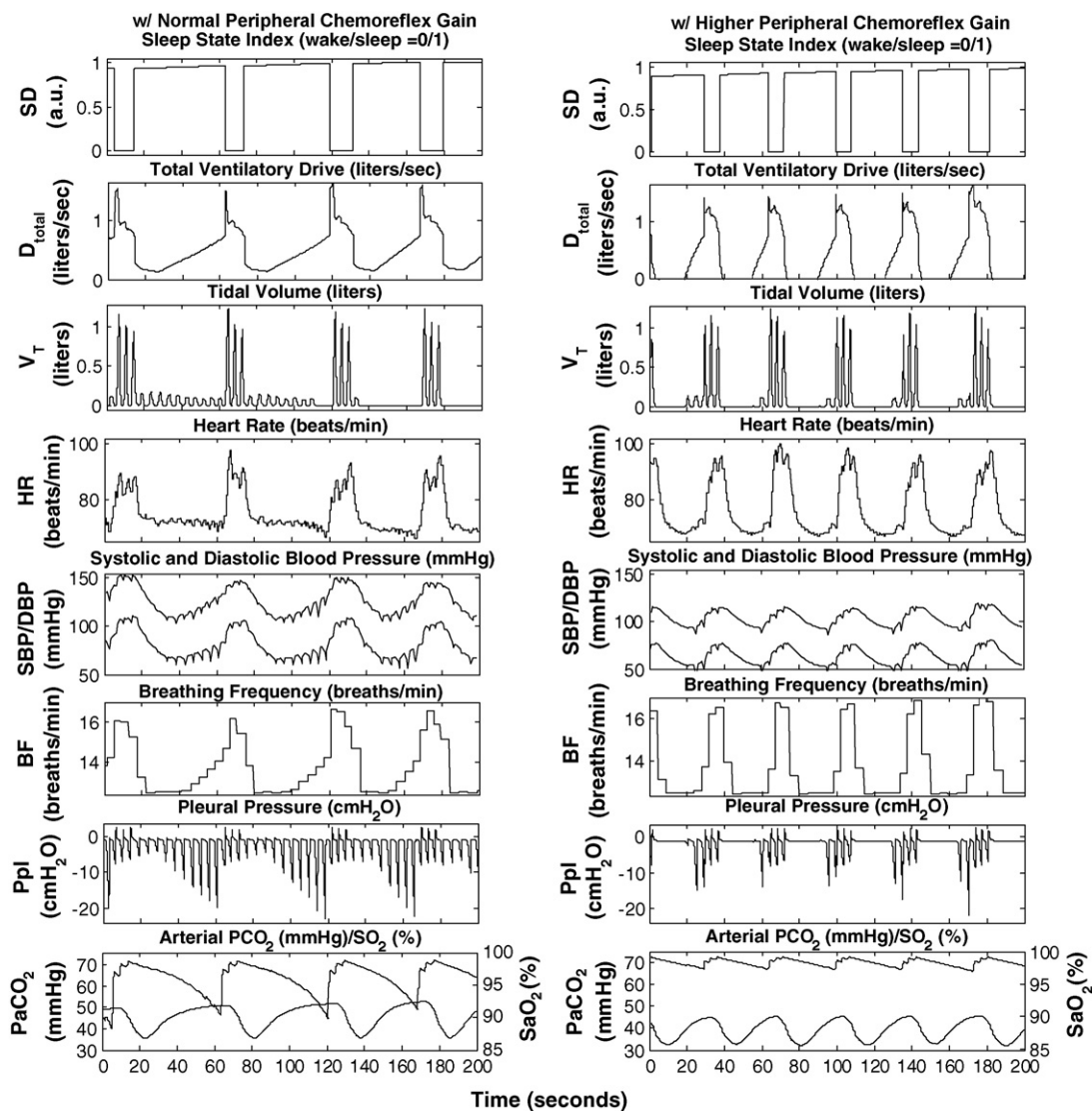


Fig. 8. Simulations showing the development of obstructive sleep apnoea following sleep onset in an OSA subject with normal chemoreflex gains (left panel) and mixed apnoea in an OSA subject with peripheral chemoreflex gain increased six fold. Time 0 represents 1800 s since the start of the simulation.

by the repetitive episodes of apnoea and arousal. Developing a quantitative dynamic model such as the one introduced here is useful for consolidating all this knowledge and providing a systematic means of predicting how the component mechanisms involved may interact under a variety of conditions. Model validation has been accomplished in two ways. First, the model has been shown to make reasonably realistic predictions of cardiovascular and respiratory control during wakefulness and sleep, consistent with a wide range of observed population-averaged physiological responses, under those conditions or interventions most pertinent to sleep-disordered breathing. Secondly, we have demonstrated the internal consistency of the simulated responses over a wide range of perturbations.

By superseding and integrating its various component subsystems – respiratory, cardiovascular, sleep–wake and autonomic nervous systems – the present model is substantially more “self-contained” relative to previous models. For instance, the cardiorespiratory model by Lu et al. (2001) requires the time-course of pleural pressure derived from experimental measurements as an input for the model to simulate the effects of the Valsalva maneuver; by contrast, in our model, the pleural pressure waveform is generated internally since the model also con-

tains all the features pertinent to respiratory mechanics and control.

4.1. Incorporation of circadian and sleep effects

The most significant difference between the present and previous models of cardiorespiratory interactions in the literature is the inclusion of a circadian and wakefulness/sleep mechanism, even though a large database of knowledge concerning the effect of sleep on the cardiovascular and respiratory systems has been developed over the past few decades. With the implemented wake/sleep mechanism, this integrative model has been able to predict the dynamic changes that occur in the cardiovascular and the respiratory systems, as well as how they interact with each other, following transitions into and out of sleep. A more surprising outcome is that this feature allows the model to predict how arousals from sleep, triggered by cardiorespiratory events during obstructive or central apnoea, affect the total duration of the sleep. This implies that constraining the total duration of sleep to remain constant would lead to the accumulation of excess sleep propensity, analogous to what is commonly referred to as “sleep debt” in the experimental literature. In its current form,

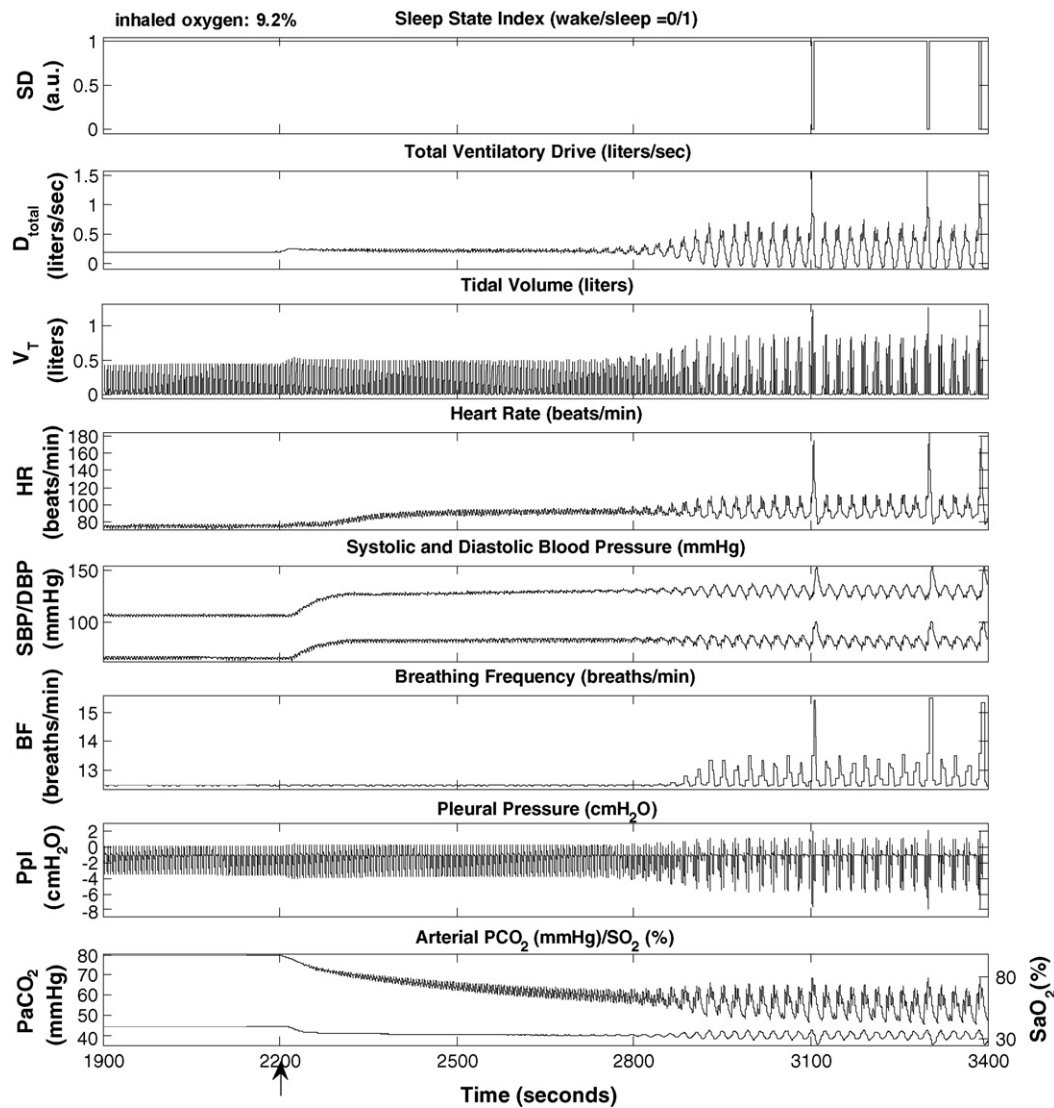


Fig. 9. Hypoxia-induced periodic breathing during sleep. Inhaled O_2 is changed from 21% to 9.2%, starting at 2200 s (arrow).

the model does not yet have the capability of directly simulating sleep debt, but this remains an important feature to add in future work.

4.2. Sensitivity analyses

As mentioned earlier, the model consists of 472 parameters, a fraction of which correspond to physiological entities and therefore are assigned values (if available) that are appropriate for the subject group and condition under study. Since this model is largely an integration of smaller submodels that have already been peer-reviewed and validated, many of the other parameters were assigned values employed in these previously published submodels. Thus, we focused on identifying the key parameters that mediate the most significant cross-interactions across the modeled subsystems and delineating them from the non-sensitive parameters that could set as constants, in order to minimize the number of free parameters that have to be modified prior to running a simulation. Sensitivity analyses were conducted to determine the relative contributions of the key parameters that played the most significant roles in various conditions. These sensitivity analyses were also useful as consistency checks. The results of the most important of these analyses are as follows:

4.2.1. Interaction between key parameters contributing to severity of obstructive sleep apnoea effects

Table 2 displays the model predictions for the sensitivity of upper airway collapsibility to state changes, S_{ua} , and the arousal threshold. In simulations of sleep in the normal subject, S_{ua} is set equal to 0.01, and during sleep, the critical closing pressure, P_{crit} , is -29.6 cmH_2O . Stable sleep is achieved and thus the arousal index (AI) is zero. The fluctuations in heart period are consistent with normal respiratory sinus arrhythmia, while the fluctuations in SBP and DBP are due primarily to the mechanical effects of respiration. When S_{ua} is increased to 0.3, so that during sleep, P_{crit} becomes much less negative (-3.5 cmH_2O), representing a substantially greater degree of collapsibility in the upper airway – but no apnoeas or arousals occur at this stage. However, when S_{ua} is increased further to 0.38, P_{crit} becomes even less negative (-2.8 cmH_2O), and now obstructive apnoeas terminated by arousals start to occur, albeit not frequently. Increasing S_{ua} a little more (to 4) leads to greater periodicity of obstructive apnoea and arousals (AI = 18), and these are the course of substantially larger amplitudes of fluctuation in heart period, SBP and DBP. Increasing S_{ua} even further to 0.5 produces more frequent apnoea and arousals (AI = 46), but the amplitudes of the swings in heart period, SBP and DBP remain relatively constant. Increasing

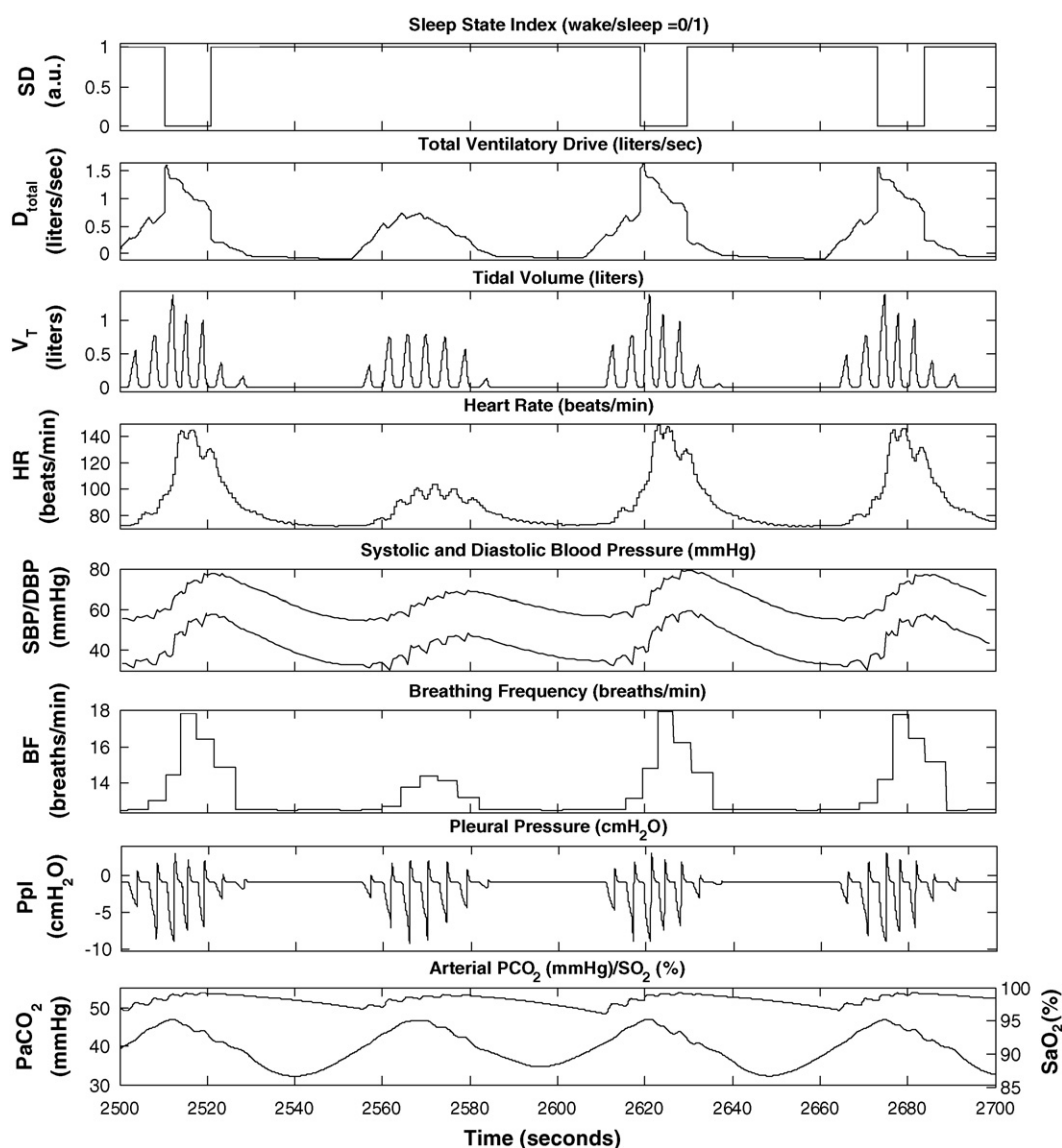


Fig. 10. Simulation of Cheyne–Stokes respiration during sleep in a subject with chronic heart failure.

Table 2

Sensitivity analysis of the effects of changing upper airway sensitivity and arousal threshold on respiratory, cardiovascular and state responses.

Sua		0.01 (control)	0.3	0.38	0.4	0.5
Arousal threshold upper limit = 0.75 (control value)	P_{crit} during sleep (cmH ₂ O)	−29.6	−3.5	−2.8	−2.7	−2.2
	AI (per hour)	0	0	1	18	46
	Δ HP (ms)	50	52	277	285	282
	Mean HP (ms)	796	790	781	768	761
	Δ SBP (mmHg)	6	4	48	52	48
	Mean SBP (mmHg)	106	107	110	120	119
	Δ DBP (mmHg)	4	12	47	51	49
Arousal threshold upper limit = 1.15	Mean DBP (mmHg)	66	67	69	77	77
	AI (per hour)	0	0	0	16	45
	Δ HP (ms)	50	52	56	302	307
	Mean HP (ms)	796	790	783	790	778
	Δ SBP (mmHg)	6	4	32	66	65
	Mean SBP (mmHg)	106	107	109	136	132
	Δ DBP (mmHg)	4	12	7	63	68
Mean DBP (mmHg)	66	67	68	87	85	

All results shown are based on 9-h overnight sleep simulations. Sua: upper airway sensitivity to changes in sleep state index; AI: arousal index; P_{crit} : critical closing pressure of the upper airway during sleep (cmH₂O); Δ HP: maximum amplitude of fluctuation in heart period (ms); Δ SDP: maximum swing in systolic blood pressure (mmHg); Δ DBP: maximum swing in diastolic blood pressure (mmHg).

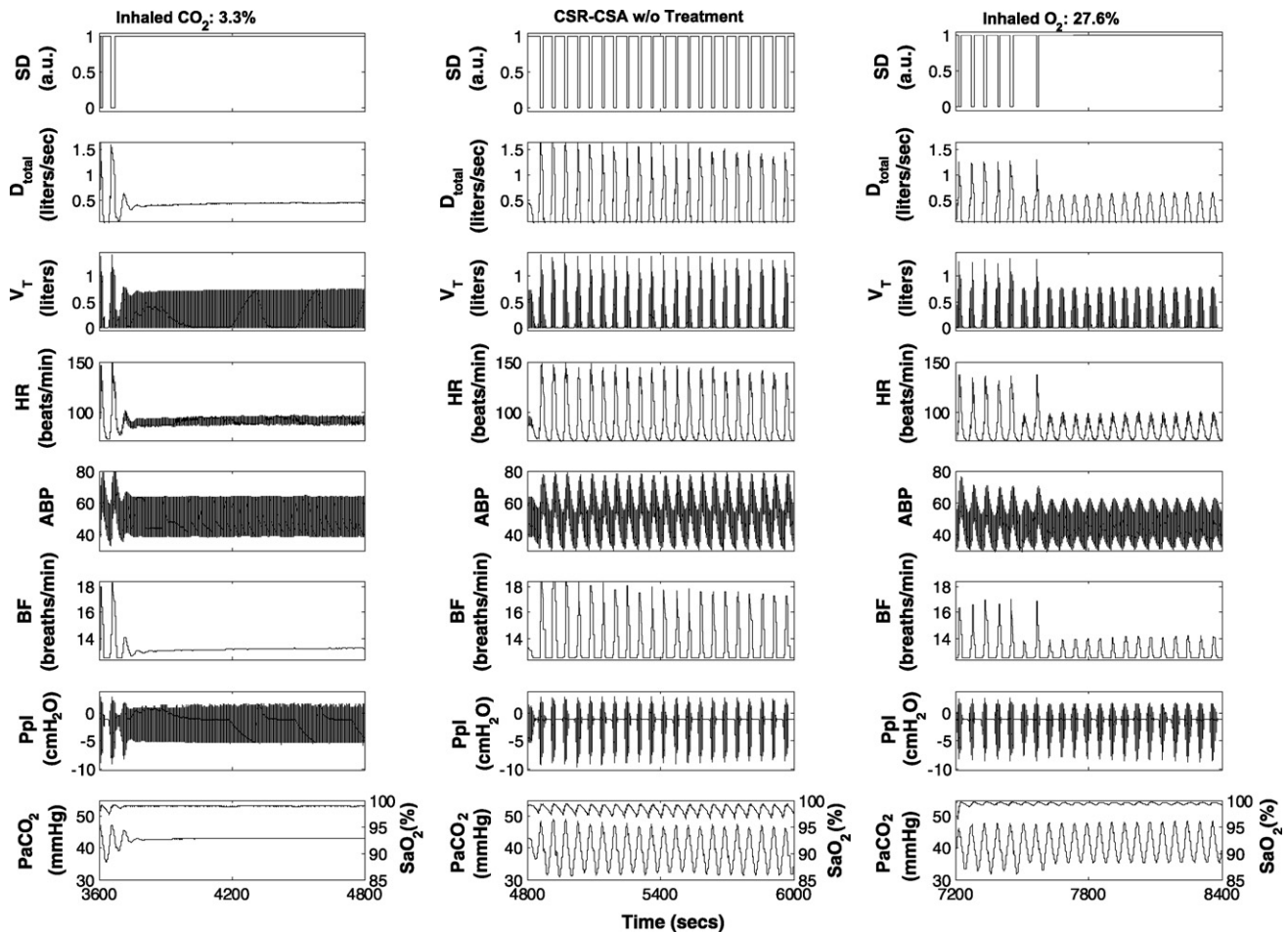


Fig. 11. Simulation of the effects of CO_2 and O_2 inhalation on a CHF subject with CSR-CSA.

the arousal threshold delays the appearance of obstructive apnoea as S_{ua} is progressively increased. For the same S_{ua} (for instance, when $S_{\text{ua}} = 0.5$), AI remains approximately the same as the case with the lower arousal threshold. However, the amplitudes of the fluctuations in heart period, SBP and DBP are substantially larger.

4.2.2. Interaction between key parameters contributing to CSR effects

Table 3 displays the results of the sensitivity analysis conducted to determine the contributions of the key parameters that influence the model during simulations of Cheyne–Stokes respiration with chronic heart failure. We have found, as might be expected, that the ability of the model to simulate CSR depends most sensitively on peripheral chemoreflex gain (G_p) and the circulation delay. However, circulation delay can be altered primarily by changing the basal value of maximum left ventricle elastance (pressure–volume ratio), E_{maxlv} , and/or the effective vascular volume between the lungs and carotid bodies. Reducing E_{maxlv} , and thus reduces cardiac contractility, increases circulation delay by decreasing cardiac output. Increasing the effective lung-to-carotid bodies vascular volume increases circulation delay for constant cardiac output. The increased vascular volume is most likely the consequence of cardiomegaly, which commonly occurs in patients with CHF.

As G_p is increased by 200% with concomitant increases in circulation delay, CSR appears but the periodic breathing pattern occurs with or without central apnoeas and without arousals. Periodic apnoeas and arousals appear when G_p is increased beyond 200%, leading to progressively higher AI with further increases in G_p . The amplitudes of the periodic fluctuations in heart period, SBP and

DBP that are entrained by the ventilatory oscillations also increase. However, with increases in G_p above 400%, the increases in these fluctuation amplitudes tend to saturate. As G_p increases, there is relatively little change in cycle duration of these oscillations.

For the same level of G_p , a reduction in E_{maxlv} produces a corresponding decrease in cardiac output and increase in circulation delay, which in turn lead to a significant increase in oscillation cycle duration. The magnitudes of these changes are relatively unaffected by the magnitude of G_p . The accompanying periodic fluctuations in heart period, SBP and DBP also increase, but these increases tend to saturate as G_p is progressively raised. AI also increases as E_{maxlv} is progressively reduced. When G_p and E_{maxlv} are kept constant while the effective vascular volume between the lungs and carotid bodies is increased, circulation delay is increased correspondingly, whereas cardiac output remains unchanged. This leads to increased AI, as well as increases in the amplitudes of fluctuations in heart period, SBP and DBP. However, at much higher levels of G_p , increased circulation delays exert considerably smaller effects on the swings in heart period and blood pressure. The overall conclusion that one can draw from this sensitivity analysis is that G_p exerts a stronger influence on the strength of the ventilatory oscillations and the amplitude of the concomitant cardiovascular oscillations that are entrained, whereas the factors that influence circulation delay bear stronger effects on oscillation cycle duration. Although not shown here, we have found that increasing central chemoreflex gain, G_c , combined with at least 30% reduction in cardiac output, can also produce CSR-CSA. However, to achieve self-sustained instability, G_c has to be increased 8-fold compared to 3-fold increase in G_p . On the other hand, if G_c and G_p are both simultaneously

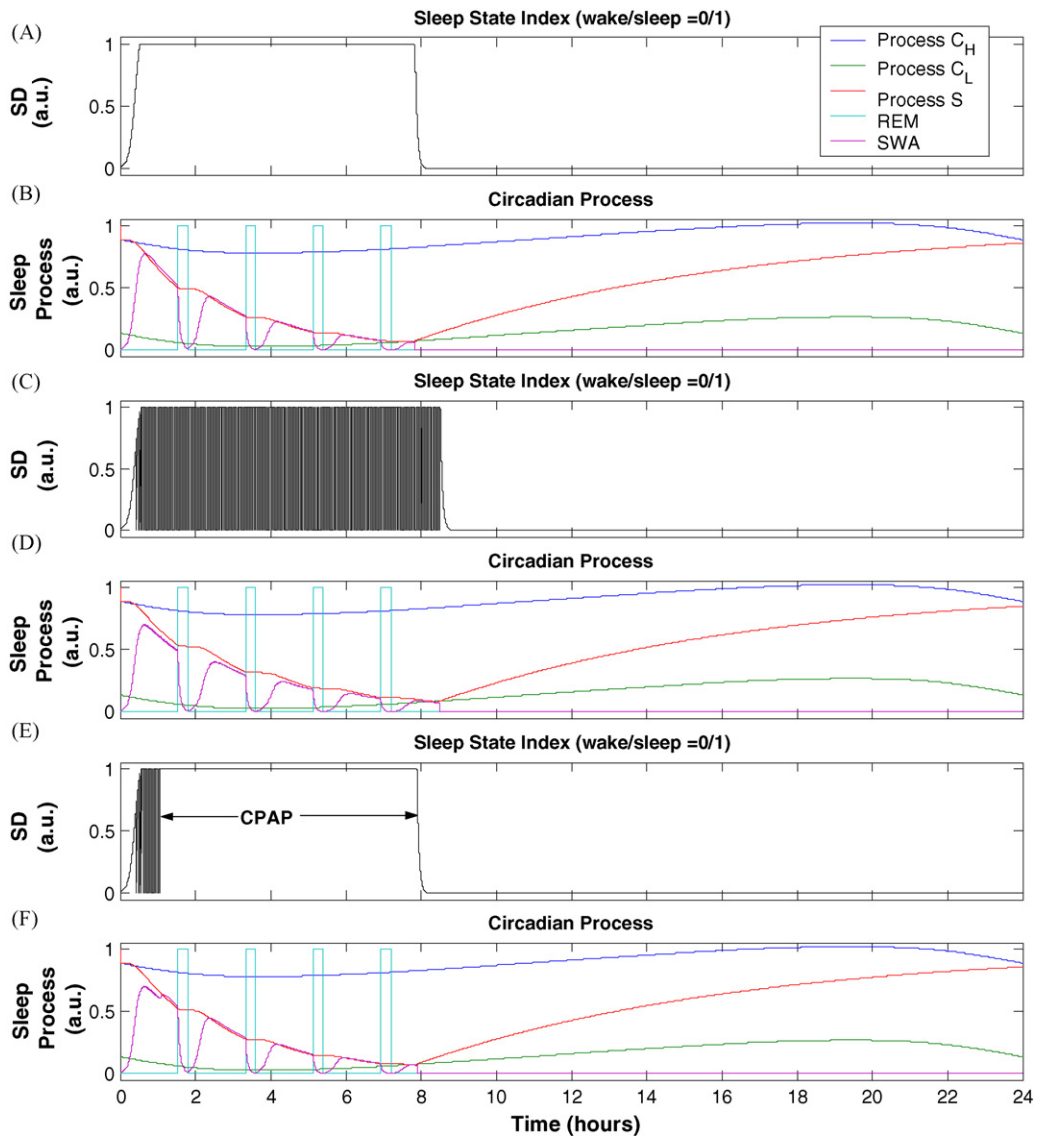


Fig. 12. Simulations with the model over a 24-h circadian cycle – comparison among different cases. Panels A and B: normal sleep; Panels C and D: OSA; Panels E and F: OSA with CPAP treatment.

increased and by the same proportion, the model remains stable. These results are compatible with the findings derived from another model (Topor et al., 2007).

4.2.3. Interaction between baroreflex and chemoreflex inputs to the ANS

Another form of sensitivity analysis consists of blocking the effects of each of the governing variables and determining the corresponding outcomes on the overall control system. This kind of approach is in fact tantamount to the experimental technique of pharmacologically or surgically eliminating the influence of specific physiological variables in order to determine their contribution to the overall system response. The example shown in Fig. 13 illustrates the competing effects of the baroreflex and chemoreflex in regulating blood pressure. In the control case, the steady state model-predicted response in blood pressure to hypoxia, induced by lowering inhaled O₂ from 21% to 8.5%, is displayed. When both baroreflex and chemoreflex inputs to the autonomic nervous system are kept intact, hypoxia elevates blood pressure by ~30%. When the baroreflex input is blocked, blood pressure is increased by ~140% relative to levels resulting from normoxia. However, when chemoreflex input is blocked while baroreflex input is restored,

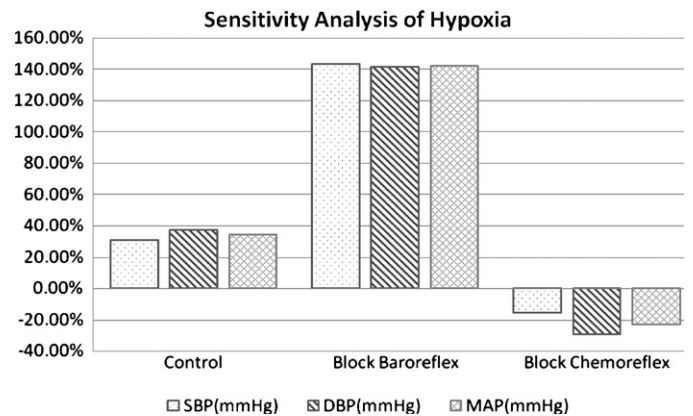


Fig. 13. Sensitivity analysis of the effects of hypoxia on blood pressure. Hypoxia is induced by lowering inhaled O₂ from 21% to 8.5%. Control: both baroreflex and chemoreflex inputs to the autonomic nervous system are left intact. "Block Baroreflex": baroreflex inputs are blocked. "Block Chemoreflex": chemoreflex inputs are blocked.

Table 3
Sensitivity analysis of key parameters that contribute to Cheyne–Stokes respiration in simulated subjects with chronic heart failure.

Model parameters ^a		Simulation results												
% Increase in Gp ^b	% Decrease in basal EmaxIV ^b	% Increase in vascular volume ^a	% Reduction in cardiac output	% Increase in circulation delay	CSR?	Central apnoea?	AI (per h)	ΔHP (ms)	Mean HP (ms)	ΔSBP (mmHg)	Mean SBP (mmHg)	ΔDBP (mmHg)	Mean DBP (mmHg)	Cycle duration (s)
0	0	0	0	0	No	No	0	42	806	3	105	3	65	N/A
200	70	20	26.73	46.73	Yes	No	0	119	777	6	82	8	52	38.4
200	90	20	42.26	62.26	Yes	Yes	0	210	716	11	65	23	43	47.4
200	70	50	27.24	77.24	Yes	No	0	181	773	23	82	16	53	42.8
200	90	50	43.11	93.11	Yes	Yes	0	226	714	10	65	13	43	52.0
400	70	20	27.99	47.99	Yes	Yes	15	396	769	22	81	26	52	40.5
400	90	20	41.66	61.66	Yes	Yes	29	422	697	24	65	28	43	48.4
400	70	50	27.97	77.97	Yes	Yes	23	403	761	24	81	28	52	45.8
400	90	50	42.19	92.19	Yes	Yes	36	437	685	26	65	30	43	56.7
600	70	20	28.37	48.37	Yes	Yes	32	403	762	22	80	27	51	44.4
600	90	20	42.56	62.56	Yes	Yes	77	430	674	24	64	28	43	49.0
600	70	50	28.80	78.80	Yes	Yes	79	410	738	25	82	29	53	48.2
600	90	50	43.44	93.44	Yes	Yes	66	443	665	27	65	32	43	57.1

All results displayed are based on 9-h overnight sleep simulations. Cp: peripheral chemoreflex gain; AI: arousal index (per hour); ΔHP: maximum amplitude of fluctuation in heart period (ms); ΔSDP: maximum amplitude of fluctuation in systolic blood pressure (mmHg); ΔDBP: maximum amplitude of fluctuation in diastolic blood pressure (mmHg).

^a Represents the model parameters.

blood pressure becomes lower than control levels (normoxia). These results demonstrate the following points: (i) stimulation of the peripheral chemoreceptors (by hypoxia) leads to sympathetic excitation which elevates blood pressure through autonomic control of the heart and peripheral vasculature; (ii) when chemoreflex inputs to the autonomic nervous system are blocked, the main effect of hypoxia on the peripheral vasculature is local vasodilation, leading to a drop in blood pressure; and (iii) the arterial baroreflex is substantially more powerful than the chemoreflex in regulating blood pressure.

4.3. Model limitations

The sleep module provides the option of generating the NREM/REM ultradian rhythm. Changes in the depth of NREM sleep are modeled as a continuous process, which likely corresponds well with the underlying physiological processes. However, we have not determined how the modeled continuous states translate into the discrete NREM sleep stages that are employed in standard polysomnography. As well, we have been overly simplistic in modeling REM stage activity and have not distinguished tonic from phasic REM. Experimental studies have found that the threshold for arousal can substantially differ between NREM and REM stages. There also appears to be a greater reduction in hypoxic ventilatory response in REM, as well as differences in many other physiological parameters, such as metabolic rate, autonomic tone, upper airway resistance and respiratory compliance. The time-courses of change in these parameters also remain unclear. These details have not been addressed in the current version of the model and further work is needed to overcome these limitations.

Other limitations include the fact that the current model is capable of simulating cardiorespiratory responses in sleep and resting wakefulness, but does not include other physiological states such as exercise, ventilatory loading or ventilation-perfusion abnormality. Although the present model does incorporate neural dynamics of the ventilatory controller in the form of short-term potentiation, other features of chemoreflex plasticity, such as hypoxic depression, or baroreflex plasticity, such as baroreflex resetting, have not been included. Presynaptic or postsynaptic gating of sensory input as a mechanism for controlling the balance of competing afferent inputs has also not been incorporated. As well, in the present model, the initiation of arousals is determined by setting ventilatory drive thresholds and the effects of arousal on respiratory and cardiovascular responses are assumed to be instantaneous. These assumptions are overly simplistic and future work could include more realistic dynamics based on empirical data.

Future improvements should provide the model with the capability of simulating different long-term disease progression scenarios (on time scales that range from days to years) with fine short-term detail (on a time scale of milliseconds). This would enable us to better understand the chronic effects of sleep-disordered breathing on autonomic function and daytime sleepiness.

Acknowledgement

This work was supported by the USC Biomedical Simulations Resource through NIH Grant EB-001978.

Appendix A. Model equations

For a summary and glossary of all variables and parameters, please see Table 1.

Respiratory gas exchange and transport**(a) Gas transport through the dead space (Khoo, 1990)**

Inspiration

$$V_{d(1)}\dot{P}_{d(1)CO_2} = \dot{V}[P_{I_{CO_2}} - P_{d(1)CO_2}] \quad (A.1a)$$

$$V_{d(i)}\dot{P}_{d(i)CO_2} = \dot{V}[P_{d(i-1)CO_2} - P_{d(i)CO_2}] \quad 2 \leq i \leq 5 \quad (A.1b)$$

$$V_{d(1)}\dot{P}_{d(1)O_2} = \dot{V}[P_{I_{O_2}} - P_{d(1)O_2}] \quad (A.2a)$$

$$V_{d(i)}\dot{P}_{d(i)O_2} = \dot{V}[P_{d(i-1)O_2} - P_{d(i)O_2}] \quad 2 \leq i \leq 5 \quad (A.2b)$$

Expiration

$$V_{d(i)}\dot{P}_{d(i)CO_2} = \dot{V}[P_{d(i+1)CO_2} - P_{d(i)CO_2}] \quad 1 \leq i \leq 4 \quad (A.3a)$$

$$V_{d(5)}\dot{P}_{d(5)CO_2} = \dot{V}[P_{ACO_2} - P_{d(5)CO_2}] \quad (A.3b)$$

$$V_{d(i)}\dot{P}_{d(i)O_2} = \dot{V}[P_{d(i+1)O_2} - P_{d(i)O_2}] \quad 1 \leq i \leq 4 \quad (A.4a)$$

$$V_{d(5)}\dot{P}_{d(5)O_2} = \dot{V}[P_{AO_2} - P_{d(5)O_2}] \quad (A.4b)$$

(b) Alveolar gas exchange (Khoo, 1990)

Inspiration

$$V_{CO_2}\dot{P}_{ACO_2} = [863\dot{Q}(C_{V_{CO_2}} - C_{A_{CO_2}}) + \dot{V}_A(P_{d(5)CO_2} - P_{ACO_2})] \quad (A.5)$$

$$V_{O_2}\dot{P}_{AO_2} = [863\dot{Q}(C_{V_{O_2}} - C_{A_{O_2}}) + \dot{V}_A(P_{d(5)O_2} - P_{AO_2})] \quad (A.6)$$

Expiration

$$V_{CO_2}\dot{P}_{ACO_2} = [863\dot{Q}(C_{V_{CO_2}} - C_{A_{CO_2}})] \quad (A.7)$$

$$V_{O_2}\dot{P}_{AO_2} = [863\dot{Q}(C_{V_{O_2}} - C_{A_{O_2}})] \quad (A.8)$$

(c) Cardiovascular mixing (heart and vasculature) (Lange et al., 1966)

$$\dot{P}_{aCO_2} = \frac{1}{(T1 \times T2)} [P_{ACO_2}(t - T_a) - (T1 + T2)\dot{P}_{aCO_2} - P_{aCO_2}] \quad (A.9a)$$

$$\dot{P}_{aO_2} = \frac{1}{(T1 \times T2)} [P_{AO_2}(t - T_a) - (T1 + T2)\dot{P}_{aO_2} - P_{aO_2}] \quad (A.9b)$$

$$T_a = \frac{LCTV}{\dot{Q}} \quad (A.10)$$

(d) Blood-gas dissociation curves (Spencer et al., 1979)CO₂

$$Ca_{CO_2} = \bar{C}a_{CO_2} \frac{F_{CO_2}^{1/a_2}}{1 + F_{CO_2}^{1/a_2}} \quad (A.11)$$

where

$$F_{CO_2} = \frac{P_{ACO_2}(1 + \beta_2 P_{AO_2})}{K_2(1 + \alpha_2 P_{AO_2})} \quad (A.12)$$

O₂

$$Ca_{O_2} = \bar{C}a_{O_2} \frac{F_{O_2}^{1/a_1}}{1 + F_{O_2}^{1/a_1}} \quad (A.13)$$

where

$$F_{O_2} = \frac{P_{AO_2}(1 + \beta_1 P_{ACO_2})}{K_1(1 + \alpha_1 P_{ACO_2})} \quad (A.14)$$

(e) Brain Compartment CO₂ exchange (Read and Leigh, 1967)

$$S_{bCO_2}\dot{P}_{bCO_2} = [MR_{bCO_2} + \dot{Q}_b S_{CO_2}(P_{aCO_2} - P_{bCO_2}) - h] \quad (A.15)$$

(f) Cerebral blood flow (Khoo, 1990)

Cerebral blood flow is calculated by solving the following quadratic equation:

$$\dot{Q}_b^2 - [1 + 0.03(P_{bCO_2} - 40)]\dot{Q}_{b0}\dot{Q}_b + 0.03(MR_{bCO_2} - h)\dot{Q}_{b0}/S_{CO_2} = 0 \quad (A.16)$$

(g) Gas exchange in the body tissues compartments (Khoo, 1990)

$$V_{tCO_2}\dot{C}_{V_{CO_2}} = [MR_{CO_2} + \dot{Q}(C_{aCO_2} - C_{V_{CO_2}})] \quad (A.17)$$

$$MR_{CO_2} = MR_{CO_2}^{awake}(0.375(1 - 0.4SI) + 0.625) \quad (A.18)$$

$$V_{tO_2}\dot{C}_{V_{O_2}} = [-MR_{O_2} + \dot{Q}(C_{aO_2} - C_{V_{O_2}})] \quad (A.19)$$

$$MR_{O_2} = MR_{O_2}^{awake}(0.375(1 - 0.4SI) + 0.625) \quad (A.20)$$

Ventilatory controller (Khoo, 1990)**(a) For normal breathing,**

$$D_{Total} = \begin{cases} Y, & TH_L \leq Y \leq TH_H \\ 0, & \text{Otherwise} \end{cases} \quad (A.21)$$

$$Y = \frac{X}{2} + \frac{X}{2} \otimes [Z_{p0} \cdot e^{-Z_{p0} \cdot t} \cdot u(t)] \quad (A.22)$$

$$X = \begin{cases} 2/(1 + e^{-5D_{Total,0}}) - 1, & D_{Total,0} > 0 \\ 0, & D_{Total,0} \leq 0 \end{cases} \quad (A.23)$$

(b) For sleep-disordered breathing,

$$D_{Total} = D_{Total,0} \quad (A.24)$$

where

$$D_{Total,0} = (1 - 0.4SI)(D_{vent} - D_{state}) \quad (A.25)$$

$$D_{state} = SI \cdot S_{wake} \quad (A.26)$$

$$D_{vent} = D_c + D_p \quad (A.27)$$

$$D_c = \begin{cases} G_c(P_{bCO_2} - I_c), & P_{bCO_2} > I_c \\ 0, & \text{Otherwise} \end{cases} \quad (A.28)$$

$$D_p = \begin{cases} G_p(P_{aCO_2} - I_{pCO_2}) \cdot (I_{pO_2} - SAO_2), & P_{aCO_2} > I_{pCO_2} \& I_{pO_2} > SAO_2 \\ 0, & \text{Otherwise} \end{cases} \quad (A.29)$$

Respiratory mechanics (Riddle and Younes, 1981)

$$P_{isom} = G_{neuromusc} D_{Total} \quad (A.30)$$

$$Y_{rs} = \frac{Y_{ua}}{1 + (R_{AW} + R_{LT} + R_{CW}) \cdot Y_{ua}} \quad (A.31)$$

Note: when $Y_{ua} = 0$, then $Y_{rs} = 0$.

$$\dot{V}_t = \frac{\sqrt{(0.25^{P_{isom}(t)e^{-V_t/0.28VC}} \cdot Y_{rs} + b^{V_t} + V_t E_{rs} Y_{rs} - P_{ao} Y_{rs})^2 + 4b^{V_t}(P_{isom} e^{-V_t/0.28VC} Y_{rs} - V_t E_{rs} Y_{rs} + P_{ao} Y_{rs})}}{2} - \frac{0.25^{P_{isom}(t)e^{-V_t/0.28VC}} \cdot Y_{rs} + b^{V_t} + V_t E_{rs} Y_{rs} - P_{ao} Y_{rs}}{2} \quad (A.32)$$

$$P_{\text{mus}} = \frac{P_{\text{isom}} e^{-V_t/0.28VC} (bV_t - 0.25\dot{V}_t)}{\dot{V}_t + bV_t} \quad (\text{A.33})$$

$$P_{\text{PL}} = R_{\text{CW}} \dot{V}_t + E_{\text{CW}} V_t - P_{\text{mus}} \quad (\text{A.34})$$

$$P_{\text{alv}} = R_{\text{LT}} \dot{V}_t + E_{\text{LT}} V_t + P_{\text{PL}} \quad (\text{A.35})$$

Upper airway mechanics

$$(P_{\text{ao}} - P_{\text{ua}}) \cdot Y_{\text{ua}} = \dot{V} - \dot{V}_{\text{ua}} \quad (\text{A.36})$$

where

$$Y_{\text{ua}} = \frac{1}{R_{\text{ua}}} \quad (\text{A.37})$$

$$P_{\text{ua}} = -\frac{P_{\text{crit}}(\text{SI})}{b_{\text{ua}}} \int \dot{V}_{\text{ua}} dt - \dot{V}_{\text{ua}} \cdot R_{\text{uaw}} \quad (\text{A.38})$$

$$Y_{\text{ua}}(\text{SI}) = k_{\text{ua}} \cdot A_{\text{ua}}, \quad \text{where } A_{\text{ua}} = \begin{cases} 0, & P_{\text{ua}} \leq P_{\text{crit}} \\ A_{0\text{ua}} \cdot (1 - P_{\text{ua}}/P_{\text{crit}}(\text{SI})), & P_{\text{crit}} < P_{\text{ua}} \leq 0 \\ A_{0\text{ua}}, & P_{\text{ua}} > 0 \end{cases} \quad (\text{A.39})$$

$$P_{\text{crit}}(\text{SI}) = \begin{cases} P_{\text{crit_awake}}, & \text{SI} = 0 \text{ (awake)} \\ P_{\text{crit_awake}}/(1 + S_{\text{ua}} \cdot (\text{SI})^2)/(1 - \text{Sleepawake}), & 0 < \text{SI} < 1 \\ P_{\text{crit_awake}}/(1 + S_{\text{ua}}), & \text{SI} = 1 \text{ (sleep)} \end{cases} \quad (\text{A.40})$$

where Sleepawake is 0 during sleep and 1 during wakefulness, S_{ua} is upper airway sensitivity and is directly related to P_{crit} .

Autonomic inputs

(a) Carotid baroreceptors (Ursino, 1998)

$$f_{\text{cs}} = \frac{f_{\text{cs,min}} + f_{\text{cs,max}} \exp((P_{\text{ABP}} - P_n + \theta_{\text{Pn}})/(k_{\text{cs}} + \theta_{\text{kcs}}))}{1 + \exp((P_{\text{ABP}} - P_n + \theta_{\text{Pn}})/(k_{\text{cs}} + \theta_{\text{kcs}}))} \quad (\text{A.41a})$$

where

$$P_{\text{ABP}} = \frac{\tau_z \cdot s + 1}{\tau_p \cdot s + 1} \cdot \text{ABP} \quad (\text{A.41b})$$

$$\theta_{\text{Pn}} = P_{\text{n.sleep}} \cdot (1 - \text{AI}) \cdot \text{SI} \quad (\text{A.41c})$$

$$\theta_{\text{kcs}} = K_{\text{cs.sleep}} \cdot (1 - \text{AI}) \cdot \text{SI} \quad (\text{A.41d})$$

(b) Chemoreceptors (Magosso and Ursino, 2001)

$$\varphi_{\text{chemo}}(Pa_{\text{O}_2}, Pa_{\text{CO}_2}) = \frac{f_{\text{chemo,max}} + f_{\text{chemo,min}} \exp((Pa_{\text{O}_2} - \overline{Pa_{\text{O}_2}}/k_{\text{chemo}}))}{1 + \exp((Pa_{\text{O}_2} - \overline{Pa_{\text{O}_2}}/k_{\text{chemo}}))} \cdot \left[K \cdot \ln \left(\frac{Pa_{\text{CO}_2}}{\overline{Pa_{\text{CO}_2}}} \right) + f_{\text{chemo,control}} \right] \quad (\text{A.42})$$

where coefficient K is defined as follows:

$$K = \begin{cases} K_H & \text{if } Pa_{\text{O}_2} > 80 \\ K_H - 1.2 \left(\frac{Pa_{\text{O}_2} - 80}{30} \right) & \text{if } 40 \leq Pa_{\text{O}_2} \leq 80 \\ K_H - 1.6 & \text{if } Pa_{\text{O}_2} < 40 \end{cases} \quad (\text{A.43})$$

$$\frac{df_{\text{chemo}}}{dt} = \frac{1}{\tau_{\text{chemo}}} (-f_{\text{chemo}} + \varphi_{\text{chemo}}) \quad (\text{A.44})$$

(c) Lung stretch receptors (Magosso and Ursino, 2001)

$$\varphi_{\text{lung}} = G_{\text{lung}} V_t \quad (\text{A.45})$$

$$\frac{df_{\text{lung}}}{dt} = \frac{1}{\tau_{\text{lung}}} (-f_{\text{lung}} + \varphi_{\text{lung}}) \quad (\text{A.46})$$

(d) Offsets (Magosso and Ursino, 2001)

$$\text{Offset}_{\text{res,vein,heart}} = \theta_{\text{san,spn,sbn}} - \theta_{\text{O}_2\text{sa,O}_2\text{sp,O}_2\text{sb}} - \theta_{\text{CO}_2\text{sa,CO}_2\text{sp,CO}_2\text{sb}} \quad (\text{A.47})$$

$$\frac{d\theta_{\text{O}_2\text{sa,O}_2\text{sp,O}_2\text{sb}}}{dt} = \frac{1}{\tau_{\text{isc}}} (-\theta_{\text{O}_2\text{sa,O}_2\text{sp,O}_2\text{sb}} + W_{\text{sa,sp,sb}}) \quad (\text{A.48})$$

$$\frac{d\theta_{\text{CO}_2\text{sa,CO}_2\text{sp,CO}_2\text{sb}}}{dt} = \frac{1}{\tau_{\text{cc}}} [-\theta_{\text{CO}_2\text{sa,CO}_2\text{sp,CO}_2\text{sb}} + g_{\text{cc,sa,sp,sb}} \cdot (P_{\text{aCO}_2} - P_{\text{aCO}_2\text{n}})] \quad (\text{A.49})$$

$$W_{\text{sa,sp,sb}} = \frac{X_{\text{sa,sp,sb}}}{1 + \exp((P_{\text{aO}_2} - P_{\text{O}_2\text{n,sa,sp,sb}})/k_{\text{isc,sa,sp,sb}})} \quad (\text{A.50})$$

Autonomic control: integration of autonomic inputs (Magosso and Ursino, 2001)

(a) Alpha-sympathetic activity

$$f_{\text{tas,res,vein}} = f_{s,\infty} + (f_{s,0} - f_{s,\infty}) \cdot \exp[k_s \cdot (-G_{\text{baro,as}} f_{\text{cs}} + G_{\text{chemo,as}} f_{\text{chemo}} - G_{\text{lung,as}} f_{\text{lung}} - G_{\text{RSA,as}} N_t - \text{Offset}_{\text{res,vein}})] \quad (\text{A.51})$$

(b) Beta-sympathetic activity

$$f_{\text{tbs}} = f_{s,\infty} + (f_{s,0} - f_{s,\infty}) \cdot \exp[k_s \cdot (-G_{\text{baro,bs}} f_{\text{cs}} + G_{\text{chemo,bs}} f_{\text{chemo}} + G_{\text{lung,bs}} f_{\text{lung}} + G_{\text{RSA,bs}} N_t - \text{Offset}_{\text{heart}})] \quad (\text{A.52})$$

(c) Parasympathetic activity

$$f_{\text{tp}} = \frac{f_{\text{para,0}} + f_{\text{para,\infty}} \cdot \exp(f_{\text{cs}} - f_{\text{cs,0}}/k_p)}{1 + \exp(f_{\text{cs}} - f_{\text{cs,0}}/k_p)} + G_{\text{chemo,p}} f_{\text{chemo}} + G_{\text{lung,p}} f_{\text{lung}} - G_{\text{RSA,p}} N_t - \text{Offset}_{\text{para,n}} \quad (\text{A.53})$$

$$\dot{N}_t = D_{\text{total}} \cdot \text{Rhythm}_{\text{respiratory}} \quad (\text{A.54})$$

Autonomic control of sino-atrial node (Ursino, 1998)

$$\text{HP} = \Delta \text{HP}_{\text{bs}} + \Delta \text{HP}_{\text{p}} + \text{HP}_{\text{basal}} \quad (\text{A.55})$$

(a) Beta-sympathetic control

$$\sigma_{\text{bs}}(t) = \begin{cases} G_{\text{bs}} \cdot G_{\text{bs}}(\text{SI}) \cdot \ln[f_{\text{tbs}}(t - D_{\text{bs}}) - f_{\text{tbs,min}} + 1], & f_{\text{tbs}} \geq f_{\text{tbs,min}} \\ 0, & f_{\text{tbs}} < f_{\text{tbs,min}} \end{cases} \quad (\text{A.56})$$

$$G_{\text{bs}}(\text{SI}) = 1 - \text{SI} \cdot (1 - \text{AI}) \cdot G_{\text{bs.sleep}} \quad (\text{A.57})$$

$$\frac{d}{dt} \Delta \text{HP}_{\text{bs}} = \frac{1}{\tau_{\text{bs}}} (-\Delta \text{HP}_{\text{bs}} + \sigma_{\text{bs}}) \quad (\text{A.58})$$

(b) Parasympathetic control

$$\sigma_{\text{ps}}(t) = \frac{G_{\text{ps}}}{G_{\text{ps}}(\text{SI})} \cdot f_{\text{tp}}(t - D_{\text{ps}}) \quad (\text{A.59})$$

$$\frac{d}{dt} \Delta \text{HP}_{\text{ps}} = \frac{1}{\tau_{\text{ps}}} (-\Delta \text{HP}_{\text{ps}} + \sigma_{\text{ps}}) \quad (\text{A.60})$$

$$G_{\text{ps}}(\text{SI}) = 1 - \text{SI} \cdot (1 - \text{AI}) \cdot G_{\text{para.sleep}} \quad (\text{A.61})$$

Alpha-sympathetic control of peripheral resistance (Ursino, 1998)

$$Z_j = \begin{cases} G_j \cdot G_{as}(SI) \cdot \ln[f_{tas,i}(t - D_j) - f_{tas \min} + 1], & f_{tas,i} \geq f_{tas \min} \\ 0, & f_{tas,i} < f_{tas \min} \end{cases} \quad (A.62)$$

$$\frac{d\Delta TPR_j}{dt} = \frac{1}{\tau_j} (-\Delta TPR_j + Z_j) \quad (A.63)$$

$$TPR_j(t) = \Delta TPR_j + TPR_{j0} \quad (A.64)$$

$$G_{as}(SI) = 1 - SI \cdot (1 - AI) \cdot G_{as, \text{sleep}} \quad (A.65)$$

Local blood flow control of peripheral resistance (Magosso and Ursino, 2001)

$$G_{bp} = \frac{1}{R_{bp}} = G_{bpn} \cdot f_{\text{chemo}_b} \quad (A.66)$$

$$f_{\text{chemo}_b} = 1 + y_{O_2_b} + y_{CO_2_b} \quad (A.67)$$

$$\frac{dy_{O_2_b}}{dt} = \frac{1}{\tau_{O_2}} \left[-y_{O_2_b} - \frac{G_{O_2_b}}{G_{as}(SI)} (C_{vO_2_b} - C_{vO_2n,b}) \right] \quad (A.68)$$

$$\frac{dy_{CO_2_b}}{dt} = \frac{1}{\tau_{CO_2}} \left(-y_{CO_2_b} + \frac{1}{G_{as}(SI)} \cdot \frac{A + (B/(1 + Ce^{D \log_{10}(P_{aCO_2_b})}))}{A + (B/(1 + Ce^{D \log_{10}(P_{aCO_2n,b})}))} - 1 \right) \quad (A.69)$$

$$R_{hp, mp} = R_{hpn, mpn} \cdot f_{\text{chemo}_{h,m}} \quad (A.70)$$

$$f_{\text{chemo}_{h,m}} = \frac{1 + y_{CO_2_{h,m}}}{1 + y_{O_2_{h,m}}} \quad (A.71)$$

$$\frac{dy_{O_2_{h,m}}}{dt} = \frac{1}{\tau_{O_2}} \left[-y_{O_2_{h,m}} - \frac{G_{O_2_{h,m}}}{G_{as}(SI)} (C_{vO_2_{h,m}} - C_{vO_2n,h,m}) \right] \quad (A.72)$$

$$\frac{dy_{CO_2_{h,m}}}{dt} = \frac{1}{\tau_{CO_2}} \left[-y_{CO_2_{h,m}} + G_{as}(SI) \cdot \frac{1 - e^{(P_{aCO_2_{h,m}} - P_{aCO_2n,h,m})/k_{CO_2_{h,m}}}}{1 + e^{(P_{aCO_2_{h,m}} - P_{aCO_2n,h,m})/k_{CO_2_{h,m}}}} \right] \quad (A.73)$$

Sleep mechanism (Achermann and Borbely, 2003; Khoo, 1990)

Process C:

$$C_{H/L} = A[0.97 \sin \theta + 0.22 \sin(2\theta) + 0.07 \sin(3\theta) + 0.03 \sin(4\theta) + 0.001 \sin(5\theta)] + X \quad \text{where } A = 0.12, \quad X = X_H = 0.9 \quad (A.74)$$

for C_H , $X = X_L = 0.15$ for C_L .

Process S:

$$\text{Awake state } (S \geq C_L) : S(t) = 1 - [1 - S(t - \Delta t)]e^{(-0.055\Delta t/3600)} \quad (A.75)$$

$$\text{Sleep state } (S \leq C_H) : \frac{dS}{dt} = -\alpha_{gc} \cdot SWA \quad (A.76)$$

$$\frac{dSWA}{dt} = \alpha_{rc} \cdot SWA \left(1 - \frac{SWA}{S} \right) - \alpha_{rc} \cdot SWA \cdot REMT(t) + SWA \cdot n(t) \quad (A.77)$$

$$REMT(t) = REM + 0.2 \cdot AI \quad (A.78)$$

$$REM = \begin{cases} 1 & \text{REM} \\ 0 & \text{NREM} \end{cases} \quad (A.79)$$

$$AI = \begin{cases} 1, & D_{\text{Total}} > \text{Thre} \\ 0, & \text{Otherwise} \end{cases}, \quad \text{where } \text{Thre} = I_{\text{vent}}(0.7 + 0.3S_{SWA}) \quad (A.80)$$

$$S_{SWA} = 1.2 \cdot \frac{SWA}{S} \quad (A.81)$$

$$D_{\text{state}} = SI = \begin{cases} S_{SWA}, & \text{sleep onset transition} \\ S_{SWA} \text{ combined}, & \text{sleep} \\ 0, & \text{awake} \end{cases} \quad (A.82)$$

$$S_{SWA} \text{ combined} = \begin{cases} 1, & AI = 0 \\ 0, & AI = 1 \end{cases} \quad (A.83)$$

References

- Achermann, P., Borbely, A.A., 2003. Mathematical models of sleep regulation. *Front. Biosci.* 8, s683–s693.
- Andreas, S., Hagenah, G., Moller, C., Werner, G.S., Kreuzer, H., 1996. Cheyne–Stokes respiration and prognosis in congestive heart failure. *Am. J. Cardiol.* 78, 1260–1264.
- Bai, J., Lu, H., Zhang, J., Zhou, X., 1997. Simulation study of the interaction between respiration and the cardiovascular system. *Methods Inf. Med.* 36, 261–263.
- Bannister, R., 1980. Defective baroreflex function in autonomic failure. In: Sleight, P. (Ed.), *Arterial Baroreceptors and Hypertension*. Oxford University Press, Oxford, UK, pp. 117–122.
- Baust, W., Bohnert, B., 1969. The regulation of heart rate during sleep. *Exp. Brain Res.* 7, 169–180.
- Berry, R.B., Asyali, M.A., McNellis, M.I., Khoo, M.C., 1998. Within-night variation in respiratory effort preceding apnea termination and EEG delta power in sleep apnea. *J. Appl. Physiol.* 85, 1434–1441.
- Berry, R.B., Gleeson, K., 1997. Respiratory arousal from sleep: mechanisms and significance. *Sleep* 20, 654–675.
- Berssenbrugge, A., Dempsey, J., Iber, C., Skatrud, J., Wilson, P., 1983. Mechanisms of hypoxia-induced periodic breathing during sleep in humans. *J. Physiol.* 343, 507–526.
- Borbely, A.A., Achermann, P., 2000. Sleep homeostasis and models of sleep regulation. In: Kogger, M.H., Roth, T., Dement, W.C. (Eds.), *Principles and Practice of Sleep Medicine*. Saunders W.B., Philadelphia.
- Bradley, T.D., Floras, J.S., 2003a. Sleep apnea and heart failure. Part I. Obstructive sleep apnea. *Circulation* 107, 1671–1678.
- Bradley, T.D., Floras, J.S., 2003b. Sleep apnea and heart failure. Part II. Central sleep apnea. *Circulation* 107, 1822–1826.
- Coleman, T.G., Randall, J.E., 1983. HUMAN. A comprehensive physiological model. *Physiologist* 26, 15–21.
- Cooper, V.L., Pearson, S.B., Bowker, C.M., Elliott, M.W., Hainsworth, R., 2005. Interaction of chemoreceptor and baroreceptor reflexes by hypoxia and hypercapnia—a mechanism for promoting hypertension in obstructive sleep apnoea. *J. Physiol.* 568, 677–687.
- Daan, S., Beersma, D.G., Borbely, A.A., 1984. Timing of human sleep: recovery process gated by a circadian pacemaker. *Am. J. Physiol.* 246, R161–R183.
- Dempsey, J.A., Smith, C.A., Eastwood, P.R., Wilson, C.R., Khoo, M.C.K., 2002. Sleep induced respiratory instabilities. In: Pack, A.I. (Ed.), *Sleep Apnea Pathogenesis, Diagnosis and Treatment*. Dekker M., New York.
- Dickinson, C., 1977. A Computer Model of Human Respiration. University Park Press, Baltimore.
- Duffin, J., Mohan, R.M., Vasilou, P., Stephenson, R., Mahamed, S., 2000. A model of the chemoreflex control of breathing in humans: model parameters measurement. *Respir. Physiol.* 120, 13–26.
- Fox, I.J., Crowley Jr., W.P., Grace, J.B., Wood, E.H., 1966. Effects of the Valsalva maneuver on blood flow in the thoracic aorta in man. *J. Appl. Physiol.* 21, 1553–1560.
- Grodins, F.S., Gray, J.S., Schroeder, K.R., Norins, A.L., Jones, R.W., 1954. Respiratory responses to CO₂ inhalation; a theoretical study of a nonlinear biological regulator. *J. Appl. Physiol.* 7, 283–308.
- Grodins, F.S., 1959. Integrative cardiovascular physiology: a mathematical synthesis of cardiac and blood vessel hemodynamics. *Q. Rev. Biol.* 34, 93–116.
- Horner, R.L., Brooks, D., Kozar, L.F., Tse, S., Phillipson, E.A., 1995. Immediate effects of arousal from sleep on cardiac autonomic outflow in the absence of breathing in dogs. *J. Appl. Physiol.* 79, 151–162.
- Huang, Y., Malhotra, A., White, D.P., 2005. Computational simulation of human upper airway collapse using a pressure-/state-dependent model of genioglossal muscle contraction under laminar flow conditions. *J. Appl. Physiol.* 99, 1138–1148.
- Javaheri, S., 1999. A mechanism for central sleep apnea in patients with heart failure. *N. Engl. J. Med.* 341, 949–954.
- Khoo, M.C., 1990. A model-based evaluation of the single-breath CO₂ ventilatory response test. *J. Appl. Physiol.* 68, 393–399.
- Khoo, M.C., Anholm, J.D., Ko, S.W., Downey 3rd, R., Powles, A.C., Sutton, J.R., Houston, C.S., 1996a. Dynamics of periodic breathing and arousal during sleep at extreme altitude. *Respir. Physiol.* 103, 33–43.
- Khoo, M.C., Gottschalk, A., Pack, A.I., 1991. Sleep-induced periodic breathing and apnea: a theoretical study. *J. Appl. Physiol.* 70, 2014–2024.
- Khoo, M.C., Koh, S.S., Shin, J.J., Westbrook, P.R., Berry, R.B., 1996b. Ventilatory dynamics during transient arousal from NREM sleep: implications for respiratory control stability. *J. Appl. Physiol.* 80, 1475–1484.
- Khoo, M.C., Yamashiro, S., 1989. Models of control of breathing. In: *Respiratory Physiology: An Analytical Approach*. Marcel Dekker, New York.
- Kirby, D.A., Verrier, R.L., 1989. Differential effects of sleep stage on coronary hemodynamic function. *Am. J. Physiol.* 256, H1378–H1383.
- Koehler, R.C., McDonald, B.W., Krasney, J.A., 1980. Influence of CO₂ on cardiovascular response to hypoxia in conscious dogs. *Am. J. Physiol. Heart Circ. Physiol.* 239, H545–H558.
- Kontos, H.A., Levasseur, J.E., Richardson, D.W., Mauck, H.P., Patterson, J.L., 1967. Comparative circulatory responses to systemic hypoxia in man in anesthetized dog. *J. Appl. Physiol.* 23, 381–386.
- Lanfranchi, P., Somers, V.K., 2001. Obstructive sleep apnea and vascular disease. *Respir. Res.* 2, 315–319.
- Lange, R.L., Horgan, J.D., Botticelli, J.T., Tsagaris, T., Carlisle, R.P., Kuida, H., 1966. Pulmonary to arterial circulatory transfer function: importance in respiratory control. *J. Appl. Physiol.* 21, 1281–1219.

- Leung, R.S., Bowman, M.E., Diep, T.M., Lorenzi-Filho, G., Floras, J.S., Bradley, T.D., 2005. Influence of Cheyne–Stokes respiration on ventricular response to atrial fibrillation in heart failure. *J. Appl. Physiol.* 99, 1689–1696.
- Leung, R.S., Bradley, T.D., 2001. Sleep apnea and cardiovascular disease. *Am. J. Respir. Crit. Care Med.* 164, 2147–2165.
- Liang, F.Y., Liu, H., 2006. Simulation of hemodynamic responses to the Valsalva maneuver: an integrative computational model of the cardiovascular system and the autonomic nervous system. *J. Physiol. Sci.* 56, 45–65.
- Lorenzi-Filho, G., Dajani, H.R., Leung, R.S.T., Floras, J.S., Bradley, T.D., 1999a. Entrapment of blood pressure and heart rate oscillations by periodic breathing. *Am. J. Respir. Crit. Care Med.* 159, 1147–1154.
- Lorenzi-Filho, G., Rankin, F., Bies, I., Bradley, T.D., 1999b. Effects of inhaled carbon dioxide and oxygen on Cheyne–Stokes respiration in patients with heart failure. *Am. J. Respir. Crit. Care Med.* 159, 1490–1498.
- Lu, K., Clark Jr., J.W., Ghorbel, F.H., Ware, D.L., Bidani, A., 2001. A human cardiopulmonary system model applied to the analysis of the Valsalva maneuver. *Am. J. Physiol. Heart Circ. Physiol.* 281, H2661–2679.
- Madwed, J.B., Albrecht, P., Mark, R.G., Cohen, R.J., 1989. Low-frequency oscillations in arterial pressure and heart rate: a simple computer model. *Am. J. Physiol.* 256, H1573–H1579.
- Magosso, E., Ursino, M., 2001. A mathematical model of CO₂ effect on cardiovascular regulation. *Am. J. Physiol. Heart Circ. Physiol.* 281, H2036–H2052.
- Mancia, G.Z.A., 1980. Cardiovascular regulation during sleep. In: Barnes, J.O.A.C.D. (Ed.), *Physiology in Sleep*. Academic Press, New York, pp. 1–55.
- McCulloch, A., Bassingthwaite, J., Hunter, P., Noble, D., 1998. Computational biology of the heart: from structure to function. *Prog. Biophys. Mol. Biol.* 69, 153–155.
- Milhorn Jr., H.T., Benton, R., Ross, R., Guyton, A.C., 1965. A mathematical model of the human respiratory control system. *Biophys. J.* 5, 27–46.
- Narkiewicz, K., Van de Borne, P.J., Pesek, C.A., Dyken, M.E., Montano, N., Somers, V.K., 1999. Selective potentiation of peripheral chemoreflex sensitivity in obstructive sleep apnea. *Circulation* 99, 1183–1189.
- Ponikowski, P., Anker, S.D., Chua, T.P., Francis, D., Banasiak, W., Poole-Wilson, P.A., Coats, A.J., Piepoli, M., 1999. Oscillatory breathing patterns during wakefulness in patients with chronic heart failure: clinical implications and role of augmented peripheral chemosensitivity. *Circulation* 100, 2418–2424.
- Read, D.J., Leigh, J., 1967. Blood–brain tissue P_{CO₂} relationships and ventilation during rebreathing. *J. Appl. Physiol.* 23, 53–70.
- Riddle, W., Younes, M., 1981. A model for the relation between respiratory neural and mechanical outputs. II. *Methods. J. Appl. Physiol.* 51, 979–989.
- Schuessler, T.F., Gottfried, S.B., Bates, J.H., 1997. A model of the spontaneously breathing patient: applications to intrinsic PEEP and work of breathing. *J. Appl. Physiol.* 82, 1694–1703.
- Somers, V.K., Dyken, M.E., Clary, M.P., Abboud, F.M., 1995. Sympathetic neural mechanisms in obstructive sleep apnea. *J. Clin. Invest.* 96, 1897–1904.
- Somers, V.K., Mark, A.L., Zavala, D.C., Abboud, F.M., 1989a. Influence of ventilation and hypocapnia on sympathetic nerve responses to hypoxia in normal humans. *J. Appl. Physiol.* 67, 2095–2100.
- Somers, V.K., Mark, A.L., Zavala, D.C., Abboud, F.M., 1989b. Contrasting effects of hypoxia and hypercapnia on ventilation and sympathetic activity in humans. *J. Appl. Physiol.* 67, 2101–2106.
- Spencer, J.L., Firouztale, E., Mellins, R.B., 1979. Computational expressions for blood oxygen and carbon dioxide concentrations. *Ann. Biomed. Eng.* 7, 59–66.
- Spicuzza, L., Porta, C., Bramanti, A., Maffei, M., Casucci, G., Casiraghi, N., Bernardi, L., 2005. Interaction between central–peripheral chemoreflexes and cerebrovascular control. *Clin. Auton. Res.* 15, 373–381.
- Stephenson, R., 2004. A theoretical study of the effect of circadian rhythms on sleep-induced periodic breathing and apnoea. *Respir. Physiol. Neurobiol.* 139, 303–319.
- Tawhai, M.H., Hunter, P., Tschirren, J., Reinhardt, J., McLennan, G., Hoffman, E.A., 2004. CT-based geometry analysis and finite element models of the human and ovine bronchial tree. *J. Appl. Physiol.* 97, 2310–2321.
- Topor, Z.L., Vasilakos, K., Younes, M., Remmers, J.E., 2007. Model based analysis of sleep disordered breathing in congestive heart failure. *Respir. Physiol. Neurobiol.* 155, 82–92.
- Ursino, M., 1998. Interaction between carotid baroregulation and the pulsating heart: a mathematical model. *Am. J. Physiol.* 275, H1733–H1747.
- Ursino, M., Magosso, E., 2000. Acute cardiovascular response to isocapnic hypoxia. I. A mathematical model. *Am. J. Physiol. Heart Circ. Physiol.* 279, H149–H165.
- Ursino, M., Magosso, E., 2003. Short-term autonomic control of cardiovascular function: a mini-review with the help of mathematical models. *J. Integr. Neurosci.* 2, 219–247.
- Verrier, R.L., Dickerson, L.W., 1991. Autonomic nervous system and coronary blood flow changes related to emotional activation and sleep. *Circulation* 83, 1181–1189.
- Wilcox, I., McNamara, S.G., Dodd, M.J., Sullivan, C.E., 1998. Ventilatory control in patients with sleep apnoea and left ventricular dysfunction: comparison of obstructive and central sleep apnoea. *Eur. Respir. J.* 11, 7–13.